

RESEARCH ARTICLE

Cascading effects augment the direct impact of CO₂ on phytoplankton growth in a biogeochemical model

Miriam Seifert^{1,*}, Cara Nissen¹, Björn Rost^{1,2}, and Judith Hauck¹

Atmospheric and oceanic CO₂ concentrations are rising at an unprecedented rate. Laboratory studies indicate a positive effect of rising CO₂ on phytoplankton growth until an optimum is reached, after which the negative impact of accompanying acidification dominates. Here, we implemented carbonate system sensitivities of phytoplankton growth into our global biogeochemical model FESOM-REcoM and accounted explicitly for coccolithophores as the group most sensitive to CO₂. In idealized simulations in which solely the atmospheric CO₂ mixing ratio was modified, changes in competitive fitness and biomass are not only caused by the direct effects of CO₂, but also by indirect effects via nutrient and light limitation as well as grazing. These cascading effects can both amplify or dampen phytoplankton responses to changing ocean pCO₂ levels. For example, coccolithophore growth is negatively affected both directly by future pCO₂ and indirectly by changes in light limitation, but these effects are compensated by a weakened nutrient limitation resulting from the decrease in small-phytoplankton biomass. In the Southern Ocean, future pCO₂ decreases small-phytoplankton biomass and hereby the preferred prey of zooplankton, which reduces the grazing pressure on diatoms and allows them to proliferate more strongly. In simulations that encompass CO₂-driven warming and acidification, our model reveals that recent observed changes in North Atlantic coccolithophore biomass are driven primarily by warming and not by CO₂. Our results highlight that CO₂ can change the effects of other environmental drivers on phytoplankton growth, and that cascading effects may play an important role in projections of future net primary production.

Keywords: Carbonate chemistry, Phytoplankton, Growth rate, Calcification, Coccolithophores, Climate change

1. Introduction

Marine primary production, mostly performed by unicellular algae (Middelburg, 2019), contributes to the global carbon cycle by the fixation of CO₂ in organic biomass via photosynthesis in the surface ocean and subsequent sinking and remineralization of biomass at depth (organic carbon pump). By the process of calcification, on the other hand, CO₂ is released into the surrounding water (carbonate pump). About half of the pelagic calcification is performed by the phytoplankton group of coccolithophores (Brownlee and Taylor, 2004; Beardall and Raven, 2013), which therefore contributes to both the organic carbon and the carbonate pump. Although their contribution to global primary production is relatively small (<10%; Poulton et al., 2007), some coccolithophore species can form large blooms that are observable from satellites (Hopkins

and Balch, 2018) and autonomous ocean profilers (Terrats et al., 2020). Locally, calcification can thereby considerably dampen the net oceanic uptake of atmospheric CO₂ (Shuttler et al., 2013).

Due to increasing anthropogenic CO₂ emissions, environmental conditions in the oceans are currently changing at an unprecedented rate, resulting in oceans that are warmer, more acidic, less oxygenated, and poorer in surface-ocean nutrients (Gruber, 2011; Kwiatkowski et al., 2020). In response to these changes, a decrease in global marine primary production (Moore et al., 2018) and shifts in species composition (e.g., Barton et al., 2016; Poloczanska et al., 2016) are expected in the future. Effects on the organic carbon and carbonate pump can already be observed locally (e.g., Bindoff et al., 2019; Pinkerton et al., 2021). For instance, observations in the North Atlantic suggest up to a 10-fold increase in coccolithophore abundance over the last decades (1965-2010, Rivero-Calle et al., 2015; 1990-2012, Krumhardt et al., 2016). Yet, the underlying reasons for this increase are not understood conclusively, with different studies suggesting either warming (Beaugrand et al., 2013) or a positive effect of dissolved CO₂ (CO_{2(aq)}; Rivero-Calle et al., 2015; Krumhardt et al.,

¹ Alfred-Wegener-Institut Helmholtz-Zentrum für Polar- und Meeresforschung, Am Handelshafen, Bremerhaven, Germany

² Universität Bremen, Bremen, Germany

* Corresponding author:
Email: miriam.seifert@awi.de

2016) as the primary cause for higher coccolithophore abundances.

Temperature, nutrient concentrations, and light availability have long been considered as the most important environmental drivers that control the magnitude of phytoplankton growth and coccolithophore calcification. However, even the carbonate system itself influences growth and calcification and becomes increasingly relevant given the current pace of ocean acidification. The impact of the carbonate system can be described with an optimum function: CO_{2(aq)} and bicarbonate (HCO₃⁻) are the primary substrates of growth and calcification (e.g., Kottmeier et al., 2014) and rising substrate levels (carbonation) can enhance growth and calcification. Rising CO_{2(aq)} concentrations result, however, in a concomitant increase in proton concentrations and thus a lower pH (acidification), which in turn eventually dampens growth and calcification (e.g., Rost and Riebesell, 2004; Gao et al., 2019). Phytoplankton species and groups differ considerably in their ability to make use of carbonation and in their sensitivity to acidification (e.g., Rost et al., 2008; Dutkiewicz et al., 2015). For instance, diatoms are affected only moderately by changes in CO_{2(aq)} and HCO₃⁻ concentrations due to their exceptionally effective CO₂ concentrating mechanisms (CCMs; Reinfelder, 2011; Pierella Karlusich et al., 2021). By diversely changing the competitive fitness of species and groups, CO₂ has also an indirect effect on phytoplankton community structure (e.g., Doney et al., 2009; Paul and Bach, 2020). Calcification, however, is particularly sensitive to ocean acidification, and laboratory experiments show that coccolithophore growth is also impacted disproportionately by increasing CO_{2(aq)} levels (Hoppe et al., 2011; Meyer and Riebesell, 2015; Zhang et al., 2019; Seifert et al., 2020). The opposing effects of carbonation and acidification lead to a transition of beneficial to detrimental impacts with increasing partial pressure of CO₂ (*p*CO₂), which has been described mechanistically by several authors (Bach et al., 2011; Bach et al., 2015; Gafar et al., 2018; Paul and Bach, 2020).

Marine biogeochemical models are important tools with predictive capabilities to understand connections and variations of biological, chemical, and biogeochemical components in space and time (e.g., Holt et al., 2014). In these models, temperature, light, and nutrients are traditionally considered as the environmental drivers to control phytoplankton growth, and very few models to date account for the effects of CO₂ on growth and calcification. Dutkiewicz et al. (2015) assessed the *p*CO₂ impact on all phytoplankton functional groups in the ecosystem model DARWIN from preindustrial to 2100 levels under the high emission scenario (RCP8.5) using different conceptual approaches based on linear, Michaelis-Menten type, and Hill type functions. They found that the picocyanobacteria *Synechococcus* and diazotrophs benefit most from increasing *p*CO₂, while the biomass of other groups, including coccolithophores and diatoms, tend to decrease. In Krumhardt et al. (2019), only coccolithophore growth was considered to be limited by low CO_{2(aq)} concentrations using a Monod function, similar to other nutrient limitations. The ratio of particulate inorganic (PIC) to organic carbon

(POC) production by coccolithophores (PIC:POC)_{cocco} and, thus, the calcite production for a given coccolithophore biomass, was defined to decrease linearly with increasing CO_{2(aq)}. Globally, model runs yielded a decrease in coccolithophore calcification by 17%, but an increase in coccolithophore growth at 900 μatm atmospheric CO₂ relative to present-day CO₂ levels. Gangsto et al. (2011) did not account for CO₂ effects on growth, but described a Michaelis-Menten-like dependence of the PIC:POC ratio on the calcite saturation state. In their model, implicit total calcification decreases by 20–60% in a high-emission scenario by the year 2100. Thus, while the CO₂ impacts on coccolithophores are not consistent across previous studies, models generally agree that increasing CO₂ can considerably alter the community structure and lead to a decrease in calcification.

None of these models, however, explicitly considers the impact of carbon speciation and the resulting two-sided carbonation-acidification effect on both growth and calcification of phytoplankton. Further, CO₂ effects on phytoplankton growth and calcification are currently largely omitted in the models of the Coupled Model Intercomparison Project (CMIP) Phase 6 (Eyring et al., 2016), which are used for the Sixth Assessment Report (AR6) of the IPCC. Besides, due to their considerable global contribution to the carbonate pump and the particular sensitivity of calcification to ocean acidification, a thorough assessment of CO₂ effects requires the implementation of coccolithophores as a separate phytoplankton group. So far, they have only been included in a few global and regional models, mainly representing the bloom-forming species *Emiliania huxleyi* (Le Quére et al., 2005; Follows et al., 2007; Gregg and Casey, 2007; Dutkiewicz et al., 2015; Kvale et al., 2015; Nissen et al., 2018; Krumhardt et al., 2019), whereas most biogeochemical models do not represent coccolithophores or calcification explicitly.

In the present study, we aim to quantify the responses of marine phytoplankton biomass and coccolithophore calcification to different atmospheric CO₂ levels and distinguish between the direct and the indirect effects of CO₂ using the physical-biogeochemical model FESOM-RECoM. First, we describe the implementation of coccolithophores and their calcification into the model. Based on a literature review of laboratory experiments, we then developed optimum functions describing the sensitivity to carbonation and acidification of growth of all modelled phytoplankton groups (coccolithophores, diatoms, small phytoplankton) and for calcification. These functions were subsequently applied in idealized simulations at preindustrial, present-day, and future atmospheric CO₂ levels. Finally, motivated by the observational studies of Beaugrand et al. (2013), Rivero-Calle et al. (2015), and Krumhardt et al. (2016), we have attempted to disentangle the effects of warming and ocean acidification on changes in global and North Atlantic coccolithophore biomass during the last decades.

2. Materials and methods

2.1. Implementing coccolithophores into RECoM

We used the global Regulated Ecosystem Model version 2 (RECoM-2-M) coupled to the Finite Element Sea Ice-Ocean

Table 1. Values of phytoplankton parameters in REcoM-2-M

Parameter ^a	Description	Units	Cocco ^b	Dia ^c	Sphy ^d
μ^{max}	Maximum growth rate constant	d ⁻¹	2.80	3.50	3.00
k^{DIN}	N half-saturation constant	mmol N m ⁻³	0.90	1.00	0.55
k^{DFe}	Fe half-saturation constant	μ mol Fe m ⁻³	0.09	0.12	0.04
k^{DSi}	Si half-saturation constant	mmol Si m ⁻³	–	4.00	–
q_{max}	Maximum N:C ratio	mol N (mol C) ⁻¹	0.15	0.20	0.20
q_{min}	Minimum N:C ratio	mol N (mol C) ⁻¹	0.04	0.05	0.05
q_{max}^{Si}	Maximum Si:C ratio	mol Si (mol C) ⁻¹	–	0.80	–
q_{min}^{Si}	Minimum Si:C ratio	mol Si (mol C) ⁻¹	–	0.04	–
σ^{DIN}	Maximum N:C uptake ratio	mmol N (mmol C) ⁻¹	0.20	0.20	0.20
σ^{DSi}	Maximum Si:C uptake ratio	mmol Si (mmol C) ⁻¹	–	0.20	–
$q_{max}^{Chl:N}$	Maximum Chl:N ratio	mg Chl (mmol N) ⁻¹	3.50	4.20	3.15
α	Initial slope of photosynthesis-irradiance curve	mmol C (mg Chl) ⁻¹ (W m ⁻² d) ⁻¹	0.10	0.19	0.14
τ_{zoo1}	Grazing preferences of first zooplankton group	dimensionless	0.666	0.083	0.250
τ_{zoo2}	Grazing preferences of second zooplankton group	dimensionless	0.5	1.0	0.5
d^{Chl}	Maximum Chl loss rate	d ⁻¹	0.50	0.50	0.50
η	Maintenance respiration rate	d ⁻¹	0.01	0.01	0.01

^aParameters relevant for the computations of growth rates are discussed in Section *Implementing coccolithophores into REcoM*.

^bCoccolithophores.

^cDiatoms.

^dSmall phytoplankton.

Model (FESOM 1.4, Schourup-Kristensen et al., 2014; Wang et al., 2014). The ocean model FESOM applies a finite element method that solves primitive hydrostatic equations on an unstructured mesh, allowing for flexible multi-resolution meshes (Sidorenko et al., 2011; Wang et al., 2014). REcoM-2-M describes the biogeochemical cycling of carbon, nitrogen, silicon, iron, and oxygen (Hauck et al., 2013; Karakuş et al., 2021). The CO₂ flux from the atmosphere to the ocean and the 3D carbonate system are computed by the mocsy 2.0 routine (Orr and Epitalon, 2015). In the previous version of the model (Karakuş et al., 2021), the ecosystem is described by two phytoplankton groups (diatoms and small-sized phytoplankton), two zooplankton groups (small, fast-growing zooplankton and slow-growing polar macrozooplankton), and two detritus groups (small, slow-sinking and large, fast-sinking particles). While the classification of diatoms is taxonomic, the small phytoplankton comprises a wide range of taxa, such as non-silicifying and non-calcifying haptophytes and green algae. In this study, we have extended the phytoplankton groups by coccolithophores, which we consider as a taxonomically separate group, similar to diatoms.

Changes in biomass result from growth and loss terms. We describe environmental impacts on growth of all phytoplankton groups, with a special focus on the parameter choice for coccolithophores. Parameters were chosen to lie

within ranges based on qualitative literature reviews, and further tuned to reproduce observed coccolithophore biomass distributions (MAREDAT dataset; O'Brien et al., 2013). While the bloom-forming coccolithophore species *E. huxleyi* is numerically the most important coccolithophore species (Paasche, 2001) and most frequently used in laboratory studies, it is not a typical representative of coccolithophores (Rost and Riebesell, 2004). Therefore, we aimed to represent the average characteristics of the diverse group of coccolithophores in our model in the parameter tuning. Subsequently, we describe the explicit implementation of coccolithophore calcification and CO₂-dependent calcite dissolution.

The growth rate GR of phytoplankton group p (coccolithophores, diatoms, or small phytoplankton) depends on the group-specific constant maximum growth rate μ^{max} (Table 1), nutrient and light limitation terms (f^N and f^L), and a temperature function (f^T):

$$GR_p = \mu_p^{max} \cdot f_p^N \cdot f_p^T \cdot f_p^L. \quad (1)$$

According to Margalef's mandala (Margalef, 1978; Wyatt, 2014), diatoms usually follow the productive r-strategy with higher growth rates, and coccolithophores the efficient K-strategy with lower growth rates. While our group of small phytoplankton includes various species that presumably cover a wide range of maximum growth rates, we assume here that the majority of coccolithophore

species, other than the bloom-forming *E. huxleyi*, are growing rather slowly and are specialized to low nutrient regions and seasons. Thus, we chose a smaller μ^{max} for coccolithophores than for diatoms and small phytoplankton in the model (**Table 1**).

Nutrient limitation f^N in Equation 1 is determined by the most limiting nutrient (dissolved inorganic nitrogen, DIN; dissolved iron, DFe; and, for diatoms, also dissolved silicic acid, DSi), and is defined as $0 \leq f^N \leq 1$ with 0 denoting strongest limitation and 1 denoting no limitation. Limitations by DIN and DSi (I^{DIN} and I^{DSi}) depend on the intracellular nitrogen or silicate to carbon quotas, and the group-specific half-saturation constants k^{DIN} and k^{DSi} (**Table 1**) for DIN and DSi, respectively (Geider et al., 1998; Hauck et al., 2013). Limitation by DFe (I^{DFe}) is described by a Michaelis-Menten function, which is dependent on the group-specific half-saturation constant k^{DFe} (**Table 1**) and the concentration of DFe in the watercolumn (i.e., $[DFe]/([DFe] + k^{DFe})$). For coccolithophores and small phytoplankton, nutrient limitation is then defined as:

$$f_p^N = \min(I_p^{DIN}, I_p^{DFe}). \quad (2)$$

Diatoms are additionally affected by DSi limitation (I^{DSi}). They have a high uptake rate at high nutrient concentrations (e.g., luxury consumption) and are less efficient under low nutrient concentrations (Sarhou et al., 2005; Litchman et al., 2007; Marañón et al., 2013). Small phytoplankton, by contrast, have the greatest ability to thrive under low nutrient conditions, e.g. due to their small cell size (Irwin et al., 2006; Marañón et al., 2013; Irion et al., 2021). Half-saturation constants k^{DIN} and k^{DFe} of coccolithophores were chosen to be smaller than those of diatoms and higher than those of small phytoplankton because their luxury consumption for nitrate is low compared to diatoms, and they are less competitive under low nutrient concentrations than other phytoplankton groups (Riegman et al., 2000; Rost and Riebesell, 2004). Literature values for maximum and minimum nitrate-to-carbon (N:C) ratios (q_{max} and q_{min}) do not show a robust difference between phytoplankton groups (Finkel et al., 2009). For diatoms and small phytoplankton, q_{max} and q_{min} (**Table 1**) translate into C:N ratios between 5 and 20, which are well in line with values reported from laboratory studies of diatoms (C:N range: 2.7–29.7; Sarhou et al., 2005). For coccolithophores, lower values result from model tuning, and q_{max} and q_{min} translate into C:N ratios between 6.6 and 25. For the temperature sensitivity f^T in Equation 1, we used a power function proposed by Fielding (2013) for coccolithophores (f_{cocco}^T), which is based on the experimental growth rate-temperature relations of *E. huxleyi* (Figure S1):

$$f_{cocco}^T = 0.1419 * T_{deg}^{0.8151}, \quad (3)$$

with T_{deg} being the temperature $\geq 0^\circ\text{C}$. At temperatures $< 0^\circ\text{C}$, the function was set to a small value (2.23×10^{-16}) rather than zero for numerical reasons. For diatoms and

small phytoplankton, f^T is defined by an Arrhenius function (Figure S1):

$$f_{Arrhenius}^T = \exp\left(-4500 \cdot \left[\frac{1}{T_K} - \frac{1}{T_{K,ref}}\right]\right), \quad (4)$$

with T_K being the temperature in K, and $T_{K,ref}$ being the reference temperature of 288.15 K (15°C). Light limitation f^L in Equation 1 is calculated as a function of the group-specific maximum light harvesting efficiency α (**Table 1**), which represents the initial slope of the photosynthesis-irradiance curve, μ^{max} (**Table 1**), photosynthetically active radiation (PAR), the variable chlorophyll-to-carbon ratio $q^{Chl:C}$, as well as nutrient limitation f^N (Equation 2) and the temperature function f^T (Equations 3 and 4; Geider et al., 1998):

$$f_p^L = 1 - \exp\left(\frac{-\alpha_p \cdot q_p^{Chl:C} \cdot PAR}{\mu_p^{max} \cdot f_p^N \cdot f_p^T}\right). \quad (5)$$

Consequently, changes in either the chlorophyll synthesis or the biomass production and the resulting alteration of $q^{Chl:C}$ affect the light limitation term. While coccolithophores are tolerant of high light levels, their ability to grow under low light conditions is lower compared to diatoms (Nielsen, 1997; Paasche, 2001; Le Quéré et al., 2005; Zondervan, 2007). In our model, coccolithophores therefore have a small maximum light harvesting efficiency α and a lower $q_{max}^{Chl:N}$ than diatoms (**Table 1**).

Loss terms of phytoplankton biomass are composed of grazing, aggregation, respiration, and excretion of dissolved organic matter. Grazing is parametrized with the Fasham formulation (Fasham et al., 1990; Vallina et al., 2014) and a variable grazing preference depending on a group-specific initial preference term and the relative contribution of each phytoplankton group to total phytoplankton biomass (Karakuş et al., 2021). We assumed that the calcite shell of coccolithophores does not serve as grazing protection (Mayers et al., 2020) and therefore chose a similar effective zooplankton grazing on coccolithophores as on small phytoplankton. We acknowledge that a protective function of the calcite shell is still under debate (e.g., Monteiro et al., 2016) and that a coccolithophore diet might reduce zooplankton growth rates by reduced digestion rates or increased swimming efforts due to the mass of the indigestible coccoliths (Haunost et al., 2021). Because the effective grazing in the model is dependent on the biomass of the respective phytoplankton group and because coccolithophore biomass is an order of magnitude smaller than small-phytoplankton biomass (see Section *Representation of coccolithophores and biogeochemical fluxes in FESOM-RECOM*), we used a higher grazing preference of the small zooplankton group on coccolithophores than on small phytoplankton (**Table 1**) to obtain a similar grazing loss of both groups. We chose the same grazing preference of the polar macrozooplankton group on coccolithophores as on small phytoplankton as its biomass is generally highest in areas with low coccolithophore biomass.

Deviating from the model version described in Hauck et al. (2013) in which calcification is performed by a constant fraction of the small phytoplankton with a fixed $(PIC:POC)_{sphy}$ ratio of 1, our model calculates calcification ($Calc_{cocco}$) depending on the specific growth rate of coccolithophores (GR_{cocco} ; Equation 1), coccolithophore biomass (C_{cocco}), and a reference PIC:POC ratio, $(PIC:POC)_{cocco}^{ref}$, that is modified by temperature ($f_{CaCO_3}^T$) and DIN limitation ($f_{CaCO_3}^N$):

$$Calc_{cocco} = GR_{cocco} \cdot C_{cocco} \cdot (PIC:POC)_{cocco}^{ref} \cdot f_{CaCO_3}^T \cdot f_{CaCO_3}^N \quad (6)$$

Here, we use a $(PIC:POC)_{cocco}^{ref}$ ratio of 1, which is motivated by a compilation of PIC:POC ratios of different coccolithophore species showing that PIC:POC ratios >1 can occur where highly calcified species like *Calcidiscus leptoporus* dominate, and PIC:POC ratios <1 can occur in the Southern Ocean if the lightly calcified *E. huxleyi* morphotype B/C dominates (Krumhardt et al., 2017). Temperature dependence of calcification $f_{CaCO_3}^T$ with decreasing $(PIC:POC)_{cocco}$ ratio at temperatures <10.6°C follows Krumhardt et al. (2017):

$$f_{CaCO_3}^T = \begin{cases} 0.104 \cdot T_{deg} - 0.108 & \text{if } T_{deg} < 10.6^\circ\text{C} \\ 1 & \text{if } T_{deg} \geq 10.6^\circ\text{C} \end{cases} \quad (7)$$

with T_{deg} being the temperature in °C. Krumhardt et al. (2017) describe the modification of the $(PIC:POC)_{cocco}$ ratio by nutrient availability using an equation of the following form:

$$f_{CaCO_3}^N = x \cdot \left(\frac{[N]}{[N] + k_{cocco}^N} + y \right) \quad (8)$$

In their study, [N] is the PO₄ concentration and k_{cocco}^N is the coccolithophore half-saturation constant for phosphate uptake. In their literature review, Krumhardt et al. (2017) found a 37% increase in $(PIC:POC)_{cocco}$ from phosphate-repleted to phosphate-limited condition, from which they derived $x = -0.48$ and $y = 1.48$ (both unitless). Because our model does not include phosphate, we adapted Equation 8 to $(PIC:POC)_{cocco}$ modification under DIN limitation, with [N] and k_{cocco}^N being the DIN concentration and coccolithophore half-saturation constant for nitrate uptake (Table 1), respectively. Krumhardt et al. (2017) also assessed the effect of nitrate limitation on $(PIC:POC)_{cocco}$, with a 25% higher ratio under nitrate-limited compared to nitrate-repleted conditions from which we derived $x = -0.31$ and $y = 1.31$.

Instead of an exponential increase with depth with a vertical length scale of 3500 m following Yamanaka and Tajika (1996) as in the previous model version (Hauck et al., 2013), calcite dissolution λ now depends on the carbonate ion concentration following Aumont et al. (2015):

$$CO_3^{2-}{}_{sat} = \frac{k_{spc}}{Ca^{2+}}, \quad (9)$$

$$\lambda = 0.197 \cdot \max\left(0, 1 - \frac{CO_3^{2-}}{CO_3^{2-}{}_{sat}}\right)^1, \quad (10)$$

with Ca^{2+} being the calcium ion concentration, k_{spc} the stoichiometric solubility product (Mucci, 1983), CO_3^{2-} the carbonate ion concentration, and $CO_3^{2-}{}_{sat}$ the saturated carbonate ion concentration. The carbonate system was computed once per week where $PAR > 1\%$ of surface PAR, and once per month where $PAR \leq 1\%$ of surface PAR to increase computational efficiency. To account for calcium carbonate dissolution above the carbonate saturation horizon, we introduced an additional dissolution in zooplankton guts. The acidic environment in guts of starving copepods can dissolve up to 38% of the calcite taken up by grazing (Pond et al., 1995; Jansen and Wolf-Gladrow, 2001; White et al., 2018). In addition, aragonite and high-magnesium forms of calcium carbonate have a shallower saturation horizon than calcite and contribute to upper-ocean calcium carbonate dissolution (Sabine et al., 2002; Feely et al., 2004; Barrett et al., 2014; Battaglia et al., 2016; Sulpis et al., 2021). Besides, high-CO₂ microenvironments in aggregates caused by metabolic activity of microbes can lead to calcium carbonate dissolution even above the saturation horizon (Milliman et al., 1999; Sulpis et al., 2021). Hence, we have deliberately overestimated gut dissolution with 50% of ingested calcite to account for aragonite and high-magnesium calcite dissolution that is not covered by the calcite-based dissolution formulation of Aumont et al. (2015).

2.2. CO₂ dependence for phytoplankton growth and coccolithophore calcification

For the implementation of CO₂ dependencies, we added limitation functions f^{CO_2} similar to the dependencies of other environmental drivers to Equations 1 and 6:

$$GR_p = \mu_p^{max} \cdot f_p^N \cdot f_p^T \cdot f_p^L \cdot f_p^{CO_2} \quad (11)$$

$$CaCO_3_{cocco} = GR_{cocco} \cdot C_{cocco} \cdot (PIC:POC)_{cocco}^{ref} \cdot f_{CaCO_3}^T \cdot f_{CaCO_3}^N \cdot f_{CaCO_3}^{CO_2} \quad (12)$$

Multiple concepts describing growth and calcification dependencies on the carbonate system exist in the literature (Bach et al., 2011; Bach, 2015; Bach et al., 2015; Gafar et al., 2018; Paul and Bach, 2020). Here we used the concept of Bach et al. (2015), which has been developed for coccolithophore calcification, as it can be well accommodated to our model structure. Furthermore, in contrast to the concepts of Paul and Bach (2020, modified Monod equation based on a generic proton to CO_{2(aq)} relationship) and Bach et al. (2011, modified Michaelis-Menten function depending only on $fCO_{2(aq)}$), it allows non-linear changes between carbon species concentrations. Because they are less well suited for our model structure, we refrained from using the concepts of Gafar et al. (2018, CO₂ term including temperature and light effects and interactions therein) and Bach (2015, bicarbonate to proton ratio). The concept of Bach et al. (2015) accounts for changes in the bicarbonate (HCO_3^-), CO_{2(aq)}, and proton concentrations in a modified Michaelis-Menten function:

$$f_p^{CO_2} = \frac{a \cdot HCO_3^-}{b + HCO_3^-} - \exp(-c \cdot CO_{2(aq)}) - d \cdot 10^{-pH}, \quad (13)$$

Table 2. Parameter values *a*, *b*, *c*, and *d* for phytoplankton growth rates and (PIC:POC)_{cocco} ratios, obtained by fitting Equation 13 to laboratory data from the references given in the table

Process	<i>a</i> (dimensionless)	<i>b</i> (mol kg ⁻¹)	<i>c</i> (kg mol ⁻¹)	<i>d</i> (kg mol ⁻¹)	RMSE ^a	References
Coccolithophore growth	1.109	37.67	0.3912	9.450·10 ⁶	0.15 d ⁻¹	Riebesell et al. (2000), Langer et al. (2006; 2009), Bach et al. (2015; 2011), Hoppe et al. (2011), Krug et al. (2011), Sett et al. (2014), Hermoso (2015), Müller et al. (2015), Kottmeier et al. (2016), and Feng et al. (2017)
Diatom growth	1.040	28.90	0.8778	2.640·10 ⁶	0.12 d ⁻¹	Ihnken et al. (2011), Sugie and Yoshimura (2013; 2016), Tatters et al. (2013), Trimbom et al. (2013), Barcelos e Ramos et al. (2014), Pančić et al. (2015), Wolf et al. (2018), and Li et al. (2019)
Small phytoplankton growth	1.162	48.88	0.2255	1.023·10 ⁷	0.16 d ⁻¹	Kranz et al. (2009), Garcia et al. (2013), Kim et al. (2013), Eichner et al. (2014), Hennon et al. (2014), and Hoppe et al. (2018)
Calcification (PIC:POC)	1.102	42.38	0.7079	1.343·10 ⁷	0.24 (unitless)	Riebesell et al. (2000), Langer et al. (2006; 2009), Bach et al. (2011; 2015), Hoppe et al. (2011), Krug et al. (2011), Sett et al. (2014), Müller et al. (2015), and Feng et al. (2017)

^aThe root mean square error (RMSE) determines to what extent the functions can reproduce the data, with RMSE = 0 representing a perfect fit.

with *p* indicating the CO₂ effect on phytoplankton growth (diatoms, small phytoplankton, or coccolithophores), and CaCO₃ indicating the CO₂ effect on coccolithophore calcification. Although the effect of CO₂ on phytoplankton growth and coccolithophore calcification can be either limiting (on the carbonation side) or inhibiting (on the acidification side) depending on the state of the carbonate system, we use the term “CO₂ limitation” for both in the remaining text equivalent to nutrient and light limitation.

To derive parameters in Equation 13 we used published laboratory experiments describing phytoplankton growth rates and PIC:POC ratios of coccolithophores at different *p*CO₂ levels. The collection builds on the literature review by Paul and Bach (2020), complemented by experimental data of other publications that fit our selection criteria (Table 2; for more details see Tables S1–S4). In particular, the data had to i) belong to one of our modelled phytoplankton groups, ii) report the response variable (growth rate and/or (PIC:POC)_{cocco} ratio) for at least three *p*CO₂ treatment levels, and iii) indicate the concentrations of all relevant carbonate system parameters (CO_{2(aq)}, HCO₃⁻,

and proton concentrations or pH). By including as many species, ecotypes, and strains as possible, we acknowledge intraspecific plasticity, which can alleviate the sensitivities towards changing environmental conditions (e.g., Wolf et al., 2018) and, thus, lead to more conservative estimates of CO₂-driven changes in phytoplankton growth and coccolithophore calcification.

We used the R function *nls* to fit Equation 13 with a non-linear least square estimate to the laboratory data of group-specific phytoplankton growth rates and (PIC:POC)_{cocco} ratios. We forced the functions through the origin to constrain the lower end of the curve to reasonable values (i.e., preventing the fit to yield positive growth or calcification when concentrations of inorganic carbon are zero). Prior to that, experimental growth rates and (PIC:POC)_{cocco} ratios were normalized, with the highest value within each dataset being scaled to 1. Because these values are reached over a wide range of carbonate species concentrations, fitted functions yielding a maximum value of 1 is not possible mathematically. To obtain functions that are non-limiting (i.e., reach a value of 1) at ideal

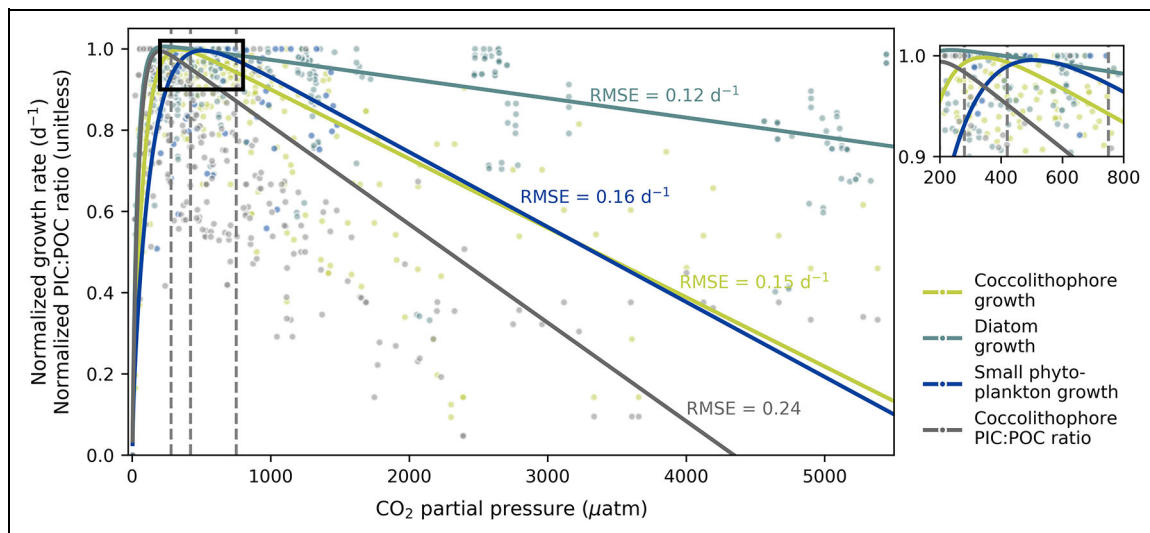


Figure 1. Reaction norms of phytoplankton growth rates and (PIC:POC)_{cocco} ratios. Point markers indicate normalized phytoplankton growth rates and (PIC:POC)_{cocco} ratios from laboratory experiments (see references in **Tables 2** and S1–S4), and lines indicate fitted functions for growth rates of coccolithophores, diatoms, and small phytoplankton, as well as (PIC:POC)_{cocco} ratios. They are exemplarily displayed for a carbonate system ranging from 3 to 5500 $\mu\text{atm } p\text{CO}_2$ and a constant alkalinity of 2300 $\mu\text{mol kg}^{-1}$ (computed with ScarFace web version 1.3.0, https://raitzsch.shinyapps.io/scarface_web/ as in Gattuso et al. [2019], and Raitzsch and Gattuso [2020], assuming surface pressure, salinity of 35, temperature of 20°C, and zero silicate and phosphate concentrations). Root mean square errors reveal the reproducibility of the data by the fitted functions. Vertical lines denote $p\text{CO}_2$ levels of the simulations (280, 420, and 750 μatm). The black inset in the main plot indicates the area enlarged on the right side. PIC = particulate inorganic carbon; POC = particulate organic carbon.

conditions, we forced the functions through the median that was obtained from the inorganic carbon species concentrations at the maximum growth rate or (PIC:POC)_{cocco} ratio of each dataset. To test whether the fitted functions would be biased by extreme $p\text{CO}_2$ levels tested in some experiments (up to 5500 μatm), we also fitted the function only through data points below 2000 and 1000 μatm , respectively (Figure S2). In both cases, growth and (PIC:POC)_{cocco} were more sensitive to increasing $p\text{CO}_2$, showing that including extreme $p\text{CO}_2$ levels does not exacerbate but softens the impact of CO₂ on growth and calcification. Hence, we selected the functions that were fitted over the entire $p\text{CO}_2$ range. Parameter values resulting from the function fits are listed in **Table 2**. Because the fits were deducted from experimental carbonate system environments, extreme carbonate system environments in the model, e.g. in the Arctic Ocean with freshwater influence, resulted in carbonate system sensitivities >1 . For the implementation in REcoM-2-M, we limited the resulting term to be ≤ 1 to prevent the carbonate system from enhancing growth and calcification to more than the pre-set maximum value.

Figure 1 displays the function fits for a sample matrix of bicarbonate, CO_{2(aq)}, and proton concentrations. Calcification and diatom growth benefit strongest from increasing $p\text{CO}_2$ at very low levels due to the carbonation effect (**Figure 1**). The steep increase in diatom growth rate already at low $p\text{CO}_2$ is well in line with the presence of effective and highly regulated CCMs in the group of diatoms (Reinfelder, 2011; Pierella Karlusich et al., 2021). The relatively stable diatom growth rate over a wide $p\text{CO}_2$

range after the steep initial increase displayed in our function can mirror the reallocation of energy, which is saved due to downregulation of CCMs under higher CO_{2(aq)} and bicarbonate availability (Shi et al., 2019). The increment from preindustrial (280 μatm) to present-day (420 μatm) $p\text{CO}_2$ levels increases the growth rate of small phytoplankton, whereas the growth rate of the other phytoplankton groups and the calcification rate decrease in this $p\text{CO}_2$ range. Besides, growth rates of small phytoplankton depict a relatively broad plateau close to maximum growth rates between present-day and future (750 μatm) $p\text{CO}_2$ levels (**Figure 1**). Studies show that small phytoplankton species such as *Micromonas* spp. and single trichomes of *Trichodesmium* spp. benefit from $p\text{CO}_2$ levels higher than preindustrial (Boatman et al., 2018), whereas $p\text{CO}_2$ levels higher than present-day must not necessarily trigger further stimulation in growth (Maat et al., 2014; Boatman et al., 2018; White et al., 2020). Calcification decreases most steeply after reaching an optimum at relatively low $p\text{CO}_2$ in our function (**Figure 1**), agreeing with experimental studies that reported coccolithophore calcification unambiguously to be the process most sensitive to any variability in the carbonate system, with an overall strong decrease in (PIC:POC)_{cocco} with increasing $p\text{CO}_2$ (e.g., Findlay et al., 2011; Meyer and Riebesell, 2015). In natural communities, this effect is caused by not only a decrease in calcification per cell, but also a shift from highly to less calcified coccolithophore species and morphotypes (Beaufort et al., 2011). Coccolithophore growth rates in our function initially decrease more steeply with increasing $p\text{CO}_2$ than small-phytoplankton growth rates, and are only outpaced

by small-phytoplankton growth rates at high $p\text{CO}_2$ levels (**Figure 1**). Our fits are in line with experimental studies which found coccolithophore growth to decrease most strongly with increasing $p\text{CO}_2$ (Riebesell et al., 2017; Seifert et al., 2020), with the exception of some coccolithophore strains (Meyer and Riebesell, 2015). In summary, we are confident that our fitted functions based on the concept of Bach et al. (2015) and constrained with laboratory data simulate the general response patterns of phytoplankton groups to different $p\text{CO}_2$ levels reasonably well.

2.3. Model simulations

We performed two sets of model simulations on the CORE-II mesh with higher resolved dynamic areas (up to 20 km, e.g. coastlines and equatorial belt) and coarser resolution of less dynamic areas (up to 150 km, open ocean; Sidorenko et al., 2011; Wang et al., 2014). We used the JRA-55-do reanalysis data set as atmospheric forcing in all simulations (version 1.3.1; Tsujino et al., 2018). Temperature and salinity were initialized with hydrographic data from the Polar Science Center Hydrographic Climatology (PHC 3.0; updated from Steele et al., 2001), DIN and DSi from the World Ocean Atlas (Garcia et al., 2013), and DFe from PISCES output (Aumont et al., 2003) which was corrected using observed profiles (de Baar et al., 1999; Boye et al., 2001). DIC and alkalinity were initialized from GLO-DAPv2 (Lauvset et al., 2016), and biomass from small values (2.23×10^{-5} for biomass in nitrogen units and 14.77×10^{-5} for biomass in carbon units, i.e. converted with the Redfield ratio).

In the first set of simulations, we aimed to investigate the effect of different atmospheric CO₂ concentrations on phytoplankton growth and biomass. We performed in total four model simulations without and with CO₂ dependence at present-day atmospheric CO₂ levels (PRESENT and PRESENT_CO2, respectively, 420 μatm ; **Table 3**) and with CO₂ dependence under preindustrial and future CO₂

levels (PREIND_CO2, 280 μatm , and FUTURE_CO2, 750 μatm ; **Table 3**). The simulations were forced with repeated year forcing, looping over the year 1961. We initialized DIC with preindustrial DIC for the PREIND_CO2 simulation, and with present-day DIC in all others (Lauvset et al., 2016). Each simulation was run for 32 years, and a mean over the last five years was analyzed for this study. Two additional simulations were performed to test the sensitivity of phytoplankton biomass towards the parameter choice of the CO₂ dependence by increasing and decreasing each parameter by 10% (Figure S3).

In a second set of four simulations, we aimed to disentangle the effects of warming and CO₂ on phytoplankton biomass over the period 1958 to 2019. In one simulation, both climatological and atmospheric CO₂ forcing varied inter-annually (VARCLI_VARCO2; **Table 3**) which accounts for both the radiative and the geochemical climate change effect. Further, a second simulation was forced by repeating the year 1961 for all atmospheric variables except CO₂ (CONSTCLI_VARCO2; **Table 3**), while in a third, atmospheric CO₂ was held constant at 280 μatm and all other variables varied inter-annually (VARCLI_CONSTCO2; **Table 3**). With these two simulations, we can separate the effects of the atmospheric CO₂ increase and other changing atmospheric forcing fields (air temperature, radiation, humidity, freshwater fluxes, wind). In a control simulation (CTRL; **Table 3**), both repeated year forcing of the year 1961 and constant atmospheric CO₂ were used. All simulations of the second set were started from previously spun-up model states, where the spin-ups covered the period 1850 to 1957 using JRA repeated year forcing of the year 1961 (Tsujino et al., 2018). The spin-up simulation used to initialize the VARCO2 simulations was forced with increasing atmospheric CO₂ concentration as in Friedlingstein et al. (2020), and the spin-up simulation used to initialize the CONSTCO2 simulations was forced with constant atmospheric CO₂ of 278 ppm. As these spin-ups

Table 3. List of model simulations performed in this study (description in Section *Model simulations*)

Simulation Name	CO ₂ Dependence	Atm. CO ₂ Level	Other Atm. Forcing Variables ^a	Simulation Period
<i>Set 1: Testing CO₂ effects on the mean state</i>				
PRESENT	no	420 μatm	RYF 1961 ^b	32 years
PRESENT_CO2	yes	420 μatm	RYF 1961 ^b	32 years
PREIND_CO2	yes	280 μatm	RYF 1961 ^b	32 years
FUTURE_CO2	yes	750 μatm	RYF 1961 ^b	32 years
<i>Set 2: Disentangling the effects of CO₂ and warming over the recent past</i>				
VARCLI_VARCO2	yes	historical	interannual varying	1958–2019
VARCLI_CONSTCO2	yes	280 μatm	interannual varying	1958–2019
CONSTCLI_VARCO2	yes	historical	RYF 1961 ^b	1958–2019
CTRL	yes	280 μatm	RYF 1961 ^b	1958–2019

^aOther atmospheric forcing variables are heat flux (by radiation and temperature), humidity, freshwater fluxes, and wind.

^bRYF 1961 = repeated year forcing, looping over the year 1961.

were conducted with the prior model version without coccolithophores and CO₂ dependence, we reset all biological tracers (phytoplankton and zooplankton biomass) to small initialization values, while taking advantage of the spun-up state for physical fields, carbonate chemistry and nutrients. This approach was chosen to ensure that the simulated carbonate chemistry represents the historical evolution of atmospheric CO₂. We started our analysis in year 4 of the simulations when the upper ocean ecosystem reached a quasi-equilibrium.

2.4. Datasets used in the evaluation of coccolithophores in FESOM-REcoM

Simulated coccolithophore biomass concentrations of the PRESENT and the PRESENT_CO2 simulations were evaluated with a compilation of observations of global coccolithophore biomass concentrations (MARine Ecosystem DATA dataset, MAREDAT; O'Brien et al., 2013) and literature estimates of global phytoplankton groups biomass, net primary production, and biogeochemical fluxes. Additionally, we evaluated the diatom representation in our model with the corresponding MAREDAT observational dataset (Leblanc et al., 2012). For a quantitative comparison of the model with the MAREDAT datasets, the modelled coccolithophore and diatom biomass was subsampled only for grid points with a corresponding observational grid point and, thus, does not represent the

entire modelled biomass of each group. Subsequently, biomass estimates of the model and the MAREDAT datasets were separated into oceanic biomes (Fay and McKinley, 2014) to assess the regional representation of simulated coccolithophores and diatoms compared to observations. An additional analysis of ecological niche occupations in the model compared to a statistical model of observations is described in Text S1.

3. Results

3.1. Representation of phytoplankton biomass and biogeochemical fluxes in FESOM-REcoM

To evaluate the phytoplankton representation in our model, we focus on the PRESENT simulation, which does not include the CO₂ dependence. To assess the impact of the CO₂ dependence at present-day atmospheric CO₂ levels, we then compare the PRESENT with the PRESENT_CO2 simulation. Simulated annual mean coccolithophore biomass is highest in the North Atlantic, the equatorial regions, upwelling regions, and the northern boundary of the Southern Ocean (Figure 2). It thereby resembles the distribution of diatoms except in the polar regions, where diatom biomass is highest of all three phytoplankton groups, whereas coccolithophore biomass is very small in high latitudes. Small phytoplankton biomass is more homogeneously distributed, with slightly lower biomass in the subtropical gyres and the polar regions

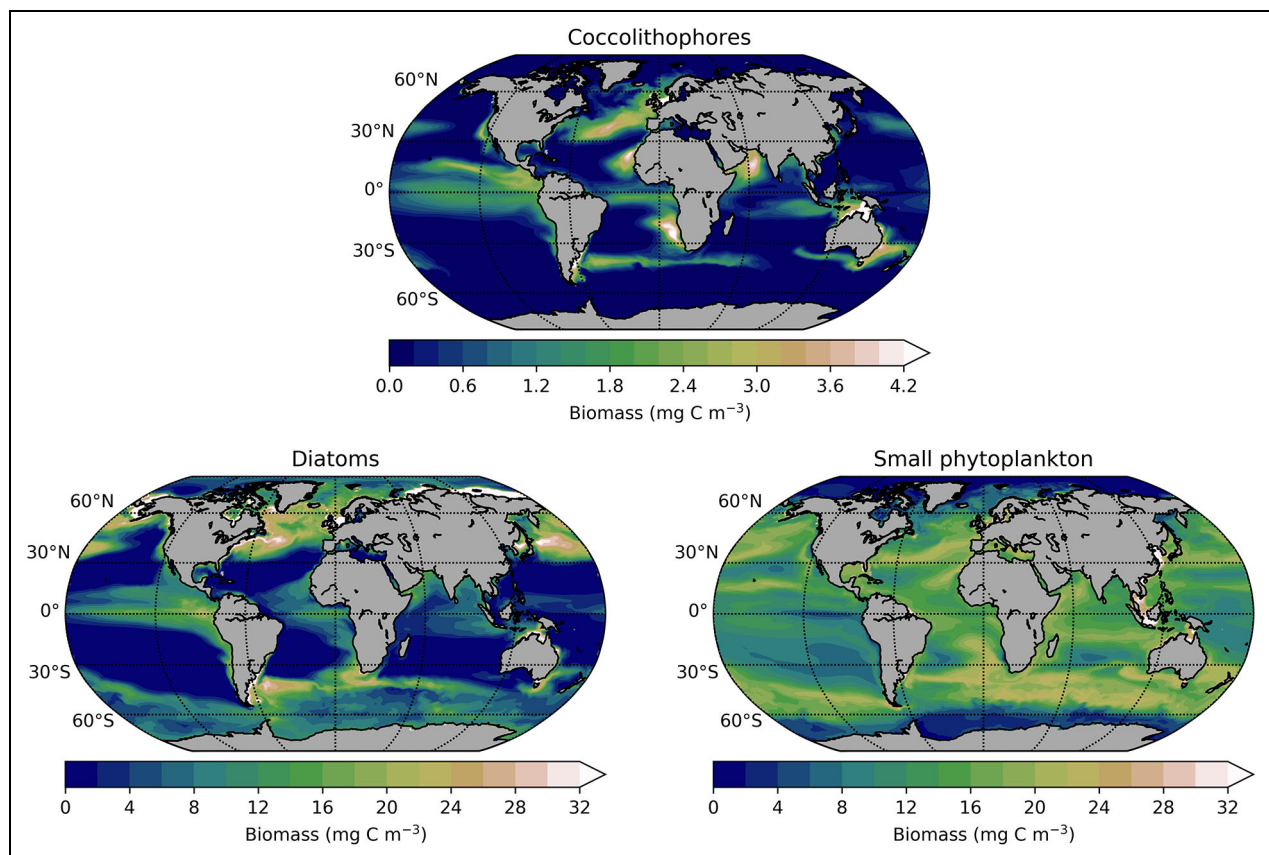


Figure 2. Mean phytoplankton biomass concentrations over the upper ocean (150 m) in the PRESENT model simulation. The PRESENT simulation does not include CO₂ dependencies of phytoplankton growth rates and coccolithophore calcification. Note the different colorscales of coccolithophores compared to diatoms and small phytoplankton.

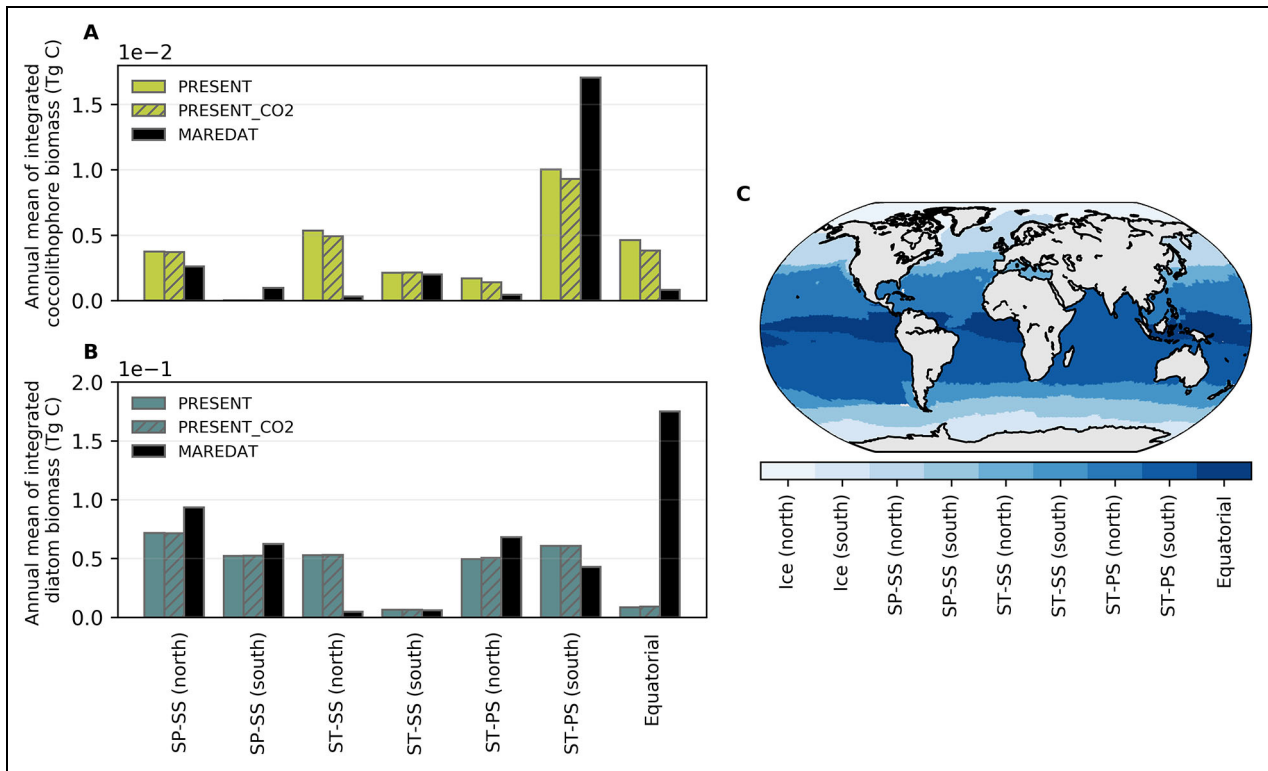


Figure 3. Representation of model-simulated coccolithophores and diatoms compared to the MAREDAT dataset. (A) Comparison of coccolithophore biomass from the PRESENT and PRESENT_CO2 simulations and the MAREDAT dataset (O’Brien et al., 2013), and (B) comparison of diatom biomass from the PRESENT and PRESENT_CO2 simulations and the MAREDAT data set (Leblanc et al., 2012) in (C) different oceanic biomes (after Fay and McKinley, 2014). Model data points were selected for available MAREDAT data points, and biomass values were integrated over the entire water column. Ice biomes (north and south) were omitted in (A) and (B) due to the negligible amount of coccolithophore biomass and low amounts of diatom biomass in both model and MAREDAT data. Model data were subsampled for locations where MAREDAT data are available and, thus, do not represent the total coccolithophore and diatom biomass in the model. SP = subpolar; ST = subtropical; SS = seasonal stratified; PS = permanently stratified.

compared to the remaining ocean. Global coccolithophore biomass is about one order of magnitude smaller than that of diatom or small phytoplankton (Figure 2).

The comparison to the MAREDAT dataset (O’Brien et al., 2013) reveals that our model overestimates coccolithophore biomass in the northern hemisphere and the equatorial region, especially in the subtropical seasonally stratified (ST-SS) north region that covers major parts of our coccolithophore patch in the North Atlantic (0.3×10^{-3} Tg C in the observations versus 5×10^{-3} Tg C in the model; Figure 3A). Modelled coccolithophore biomass in the ST-SS (south) region, covering the coccolithophore patch at the northern border of the Southern Ocean, is fairly close to observational data with about 2×10^{-3} Tg C. Because the model does not depict the coccolithophore biomass of 0.1×10^{-3} Tg C from observations further south in the subpolar seasonally stratified (SP-SS) region (Figure 3A), high coccolithophore biomass usually occurring between 40 and 60°S in the Southern Ocean (Balch et al., 2011) is shifted northwards in our model. The coccolithophore niche analysis (see Text S1 and Figure S4) reveals a good model representation of *E. huxleyi* and coccolithophore species in warm regions, while coccolithophore species in cold regions are not represented.

Diatom biomass is in the range of observational data for most regions, except for an overestimation of modelled biomass in the ST-SS (north) region and a strong underestimation in the equatorial region (Figure 3B; Leblanc et al., 2012). We attribute this underestimation to a patch with very high observed diatom biomass in the equatorial Atlantic which is not captured by the model, as well as a mismatch between high diatom biomass on the model grid and the MAREDAT grid points for which the model was sampled. For both coccolithophores and diatoms, trends in inter-biome biomass differences are similar in the grid subsampled for MAREDAT datapoints (Figure 3) and the entire model grid (Figure 2; data not shown as barplots).

Globally integrated annual mean coccolithophore biomass amounts to 0.03 Pg C, corresponding to the upper end of literature estimates (0.001–0.032 Pg C), and to 2.3% of the total simulated phytoplankton biomass (Table 4). The contribution of coccolithophores to total NPP is slightly higher in our model (3.3% of total NPP) than in literature estimates (2% of total NPP; Table 4). Diatom biomass (0.49 Pg C), silicate export (84.3 Tmol yr⁻¹), and the relative share of diatoms to total NPP (29.9%) fit well into the fairly wide range of literature estimates (0.01–0.94 Pg C, 69–185 Tmol yr⁻¹, and

Table 4. Global estimates of phytoplankton biomass (total and by group), net primary production, and global biogeochemical fluxes compared to literature estimates

Description	PRESENT	PREIND_CO2	PRESENT_CO2	FUTURE_CO2	Literature	References
<i>Biomass</i>						
Phytoplankton biomass ^a in Pg C	1.36	1.34	1.35	1.35	na ^b	⁴ O'Brien et al. (2013), observations;
Cocco in Pg C (% of total)	0.031 (2.3)	0.030 (2.3)	0.030 (2.2)	0.032 (2.4)	0.001–0.032 (0.2–2) ^{A, C}	⁵ Leblanc et al. (2012), observations;
Dia in Pg C (% of total)	0.49 (35.8)	0.52 (38.4)	0.49 (36.4)	0.50 (36.6)	0.01–0.94 (3–50) ^{B, C}	⁶ Buitenhuis et al. (2013), observations;
Sphy in Pg C (% of total)	0.84 (61.9)	0.80 (59.3)	0.83 (61.4)	0.83 (61.0)	na ^b	⁷ Cregg and Casey (2007), model study;
(PIC:POC) _{cocco} ^a (unitless)	1.2	1.1	1.1	1.1	0.7–1.4 ^{M, N, O}	⁸ Behrenfeld and Falkowski (1997), satellite data;
<i>Net primary production</i>						
Phytoplankton NPP ^a in Pg C yr ⁻¹	30.3	28.6	29.7	29.9	24–56 ^{C, D, E, F, G, H, I, J}	⁹ Buitenhuis et al. (2013), model study;
Cocco in Pg C yr ⁻¹ (% of total)	1.0 (3.3)	0.9 (3.1)	0.9 (3.1)	1.0 (3.5)	na ^b (2) ^K	¹⁰ Sinha et al. (2010), model study;
Dia in Pg C yr ⁻¹ (% of total)	9.0 (29.9)	9.4 (32.9)	9.1 (30.8)	9.2 (30.6)	na ^b (15–35) ^{K, L}	¹¹ Field et al. (1998), model study;
Sphy in Pg C yr ⁻¹ (% of total)	20.2 (66.8)	18.3 (64.0)	19.7 (66.1)	19.7 (66.0)	na ^b	¹² Schneider et al. (2008), model study;
<i>Export</i>						
Calcite export ^a (Pg C yr ⁻¹)	1.2	1.0	1.1	1.1	0.1–4.7 ^{P, Q, R, S, T, U, V*}	¹³ Carr et al. (2006), satellite data;
POC export ^a (Pg C yr ⁻¹)	4.8	4.7	4.8	4.8	5–13 ^{T, V, W, X, Y*}	¹⁴ Jin et al. (2006), model study;
Rain ratio ^a (unitless)	0.3	0.2	0.2	0.2	0.06–0.4 ^{N, Z, *}	¹⁵ Nelson et al. (1995), model study and observations (reference collection);
Silicate export ^a (Tmol Si yr ⁻¹)	84.3	84.3	84.0	85.7	69–185 ^{L, T, V, AA, BB, *}	¹⁶ Indray et al. (2011), experiments;
<i>Export</i>						
Calcite export ^a (Pg C yr ⁻¹)	1.2	1.0	1.1	1.1	0.1–4.7 ^{P, Q, R, S, T, U, V*}	¹⁷ Zondervan et al. (2001), experiments;
POC export ^a (Pg C yr ⁻¹)	4.8	4.7	4.8	4.8	5–13 ^{T, V, W, X, Y*}	¹⁸ Zondervan et al. (2002), experiments;
Rain ratio ^a (unitless)	0.3	0.2	0.2	0.2	0.06–0.4 ^{N, Z, *}	¹⁹ Lee (2001), model study;
Silicate export ^a (Tmol Si yr ⁻¹)	84.3	84.3	84.0	85.7	69–185 ^{L, T, V, AA, BB, *}	²⁰ Jin et al. (2006), model study;
<i>Export</i>						
Calcite export ^a (Pg C yr ⁻¹)	1.2	1.0	1.1	1.1	0.1–4.7 ^{P, Q, R, S, T, U, V*}	²¹ Gangsto et al. (2008), model study;
POC export ^a (Pg C yr ⁻¹)	4.8	4.7	4.8	4.8	5–13 ^{T, V, W, X, Y*}	²² Berelson et al. (2007), model study and observations;
Rain ratio ^a (unitless)	0.3	0.2	0.2	0.2	0.06–0.4 ^{N, Z, *}	²³ Dunne et al. (2007), model study and observations (reference collection);
Silicate export ^a (Tmol Si yr ⁻¹)	84.3	84.3	84.0	85.7	69–185 ^{L, T, V, AA, BB, *}	²⁴ Battaglia et al. (2016), model study;
<i>Export</i>						
Calcite export ^a (Pg C yr ⁻¹)	1.2	1.0	1.1	1.1	0.1–4.7 ^{P, Q, R, S, T, U, V*}	²⁵ Gehlen et al. (2006), model study;
POC export ^a (Pg C yr ⁻¹)	4.8	4.7	4.8	4.8	5–13 ^{T, V, W, X, Y*}	²⁶ Palevsky and Doney (2018), model study;
Rain ratio ^a (unitless)	0.3	0.2	0.2	0.2	0.06–0.4 ^{N, Z, *}	²⁷ Henson et al. (2011),
Silicate export ^a (Tmol Si yr ⁻¹)	84.3	84.3	84.0	85.7	69–185 ^{L, T, V, AA, BB, *}	²⁸ Schlitzer (2000), model study;
<i>Export</i>						
Calcite export ^a (Pg C yr ⁻¹)	1.2	1.0	1.1	1.1	0.1–4.7 ^{P, Q, R, S, T, U, V*}	²⁹ Sarmiento et al. (2002), model study;
POC export ^a (Pg C yr ⁻¹)	4.8	4.7	4.8	4.8	5–13 ^{T, V, W, X, Y*}	³⁰ Tréguer and De La Rocha (2013), observations (synthesis);
Rain ratio ^a (unitless)	0.3	0.2	0.2	0.2	0.06–0.4 ^{N, Z, *}	³¹ Tréguer et al. (2021), observations (synthesis);
Silicate export ^a (Tmol Si yr ⁻¹)	84.3	84.3	84.0	85.7	69–185 ^{L, T, V, AA, BB, *}	³² Tréguer et al. (2021), observations (synthesis);

NPP = net primary production; Cocco = coccolithophores; Dia = diatoms; Sphy = small phytoplankton; PIC = particulate inorganic carbon; POC = particulate organic carbon.

^aBiomass and NPP were integrated over the upper 150 m of the water column, export fluxes and rain ratio computed at 100 m depth, and (PIC:POC)_{cocco} calculated in the upper 50 m of the water column from all grid points with a coccolithophore biomass > 1 mg C m⁻³. Both detritus groups were used to compute export fluxes and rain ratios.

^bna = data not available from literature.

15–35%, respectively; **Table 4**). With approximately 30 Pg C yr⁻¹, total NPP in our model is at the lower end of literature estimates (**Table 4**), which can be attributed at least partly to an underestimation of small-phytoplankton productivity, given that both coccolithophore and diatom NPP are likely at the upper end, and to the absence of nitrogen fixers in our model that usually increase primary productivity in the low latitudes of the real ocean. The (PIC:POC)_{cocco} of 1.2 and the calcite export of 1.2 Pg C yr⁻¹ are well within the range of literature values (0.7–1.4 and 0.1–4.7 Pg C yr⁻¹, respectively; **Table 4**), indicating a good representation of coccolithophore calcification and calcite dissolution in the model. With 0.3, the rain ratio (PIC:POC export at 100 m) from the model is well within the very broad range of the literature estimates (0.06–1.0; **Table 4**).

In the PRESENT_CO2 simulation, coccolithophore biomass is lower in all regions compared to the PRESENT simulation, especially in the ST-SS (north), the subtropical permanently stratified (north), and the equatorial region (**Figure 3A**). This lower amount of biomass results in a smaller over-estimation of coccolithophore biomass compared to the MAREDAT dataset and, thus, in a better agreement with observations. Differences in diatom biomass between the PRESENT and the PRESENT_CO2 simulation are very small (**Figure 3B**). Global estimates of biomass, production, and export fluxes decrease slightly compared to the PRESENT simulation, but are still in the range of literature estimates (**Table 4**). Varying the parameters of the CO₂ dependencies (**Table 2**) by ±10% can change phytoplankton biomass locally by up to 10% (**Figure S3**). However, our analysis shows that the parameter set used in the PRESENT_CO2 simulation (**Table 2**), which is based on function fits to laboratory data, modifies phytoplankton biomass only little (less than 10%) compared to the PRESENT simulation. Hence, we are confident that our approach of the parameter estimation results in a good representation of present-day phytoplankton. Overall, our model represents phytoplankton biomass, distribution, and export fluxes reasonably well in both the PRESENT and the PRESENT_CO2 simulation.

3.2. Changes in phytoplankton growth, biomass, NPP, calcification, and export at different CO₂ levels

In this section, we first describe spatial patterns of changes in carbonate chemistry (**Figure 4**) and phytoplankton biomass (**Figure 5**). Direct and indirect CO₂ effects are then analyzed in four selected regions (**Figure 6**), namely the three coccolithophore key regions SP-SS + ST-SS (north), equatorial, and ST-SS (south) because of the high sensitivity of coccolithophores to CO₂ changes (**Figure 1**), and the Southern Ocean region, SP-SS + Ice (south) where the spatial comparison between the simulations reveals a considerable decrease of small phytoplankton and a concomitant increase of diatoms (**Figure 5B** and **C**). Temperature effects remain the same in all simulations and, thus, are not discussed. Global estimates of biomass and NPP are integrated over the upper 150 m of the water column. We refer to surface maps and, for the separate regions, to

absolute and relative changes at the surface, noting that relative changes are mostly in the same order of magnitude for depth-integrated properties (see **Figure S5** for depth distribution of phytoplankton biomass). If the relative changes of surface and depth-integrated biomass differ significantly, we mention them separately.

3.2.1. Preindustrial versus present-day CO₂

Phytoplankton biomass and NPP at preindustrial *p*CO₂ (280 μatm) are compared to values at present-day *p*CO₂ (420 μatm) and related to changes in carbonate chemistry. On the global scale, largest changes are observed for small phytoplankton with 2.1% lower total biomass and NPP (**Table 4**), driven primarily by changes in the equatorial and temperate zones (**Figure 5C**). This coincides with the regions of strongest reduction in surface HCO₃⁻ concentrations of up to 8% (about 160 mmol m⁻³; **Figure 4B**). An exception is the South Pacific subtropical gyre, where considerably lower surface HCO₃⁻ concentrations barely affect small-phytoplankton biomass. Total biomass and NPP of diatoms are 2.0% and 2.1% higher, respectively, with lower atmospheric CO₂ concentrations (**Table 4**), resulting mainly from changes in the same regions as for small phytoplankton (**Figure 5B**). Globally, biomass and NPP of coccolithophores differ only slightly between preindustrial and present-day *p*CO₂ (**Table 4**; **Figure 5A**). Surface CO_{2(aq)} is by about 5–10% lower in the preindustrial compared to the present-day simulation, mostly in the Arctic (up to 10 mmol m⁻³) and least in the equatorial regions, and pH is up to 0.2 units higher in the polar regions (**Figure 4A** and **C**). Alterations in total phytoplankton biomass largely follow the slightly different pattern of change in surface HCO₃⁻ as described above, while CO_{2(aq)} and pH seemingly are not the main factors for differences in phytoplankton biomass in the two simulations. The (PIC:POC)_{cocco} ratio is about the same in both simulations (**Table 4**) because spatial changes in calcite concentration follow changes in coccolithophore biomass (**Figure 5D**). POC and calcite export are slightly lower by 0.1 Pg C yr⁻¹, resulting in an unaltered rain ratio, and silicate export is 0.3 Tmol yr⁻¹ higher (**Table 4**).

In the four selected regions, direct growth responses to lower atmospheric CO₂ concentrations are not sufficient to explain the rearrangement of phytoplankton groups. Growth rates of small phytoplankton are as much as 4% lower in the SP-SS + ST-SS (north), the equatorial, and the ST-SS (south) regions at preindustrial atmospheric CO₂ (**Figure 6A, C, and E**). This reduction of the growth rates is caused by a stronger growth limitation by CO₂ and light, which is partly counteracted by weakened nutrient limitation (**Figure 4D** and **E**). Hence, small-phytoplankton biomass in these regions is 3–4% lower (0.1–0.3 Tg C). In the same regions, diatom biomass is 2–5% (0.05–0.1 Tg C) higher. Changes in their growth rates, however, are not caused by lower atmospheric CO₂ directly (**Figure 6A, C, and E**) but by the modulation of other factors. Coccolithophores are affected most in the SP-SS + ST-SS (north) region, where biomass is reduced by 14% (5% integrated over the entire watercolumn), which does not correspond

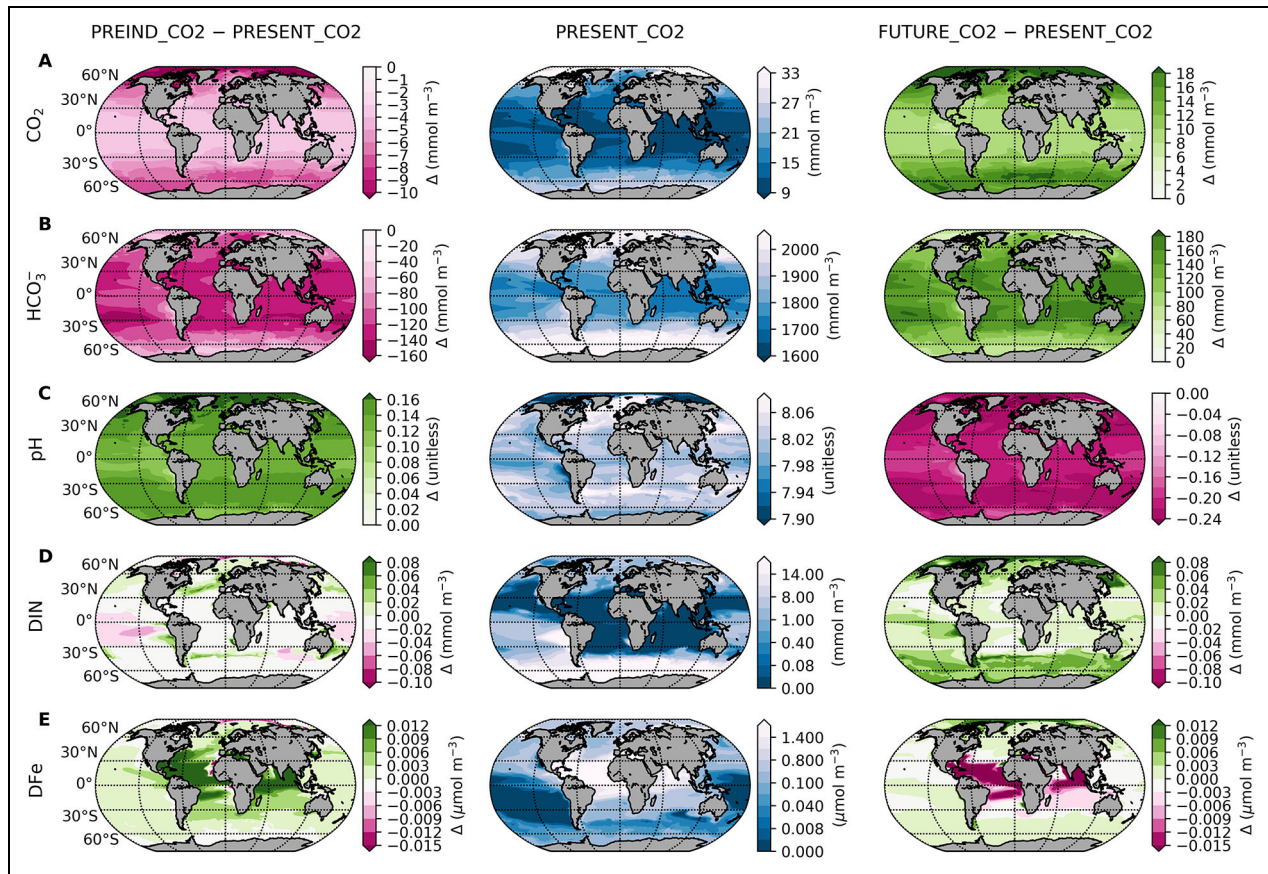


Figure 4. Surface inorganic carbonate system variables and nutrients in model simulations. Maps display (A) $\text{CO}_{2(aq)}$, (B) HCO_3^- , (C) pH, (D) dissolved inorganic nitrogen (DIN), and (E) dissolved iron (DFe) in the PRESENT_CO₂ simulation (middle column), and as total difference between the PRESENT_CO₂ simulation and the PREIND_CO₂ (left) and FUTURE_CO₂ (right), respectively (PREIND_CO₂ – PRESENT_CO₂ and FUTURE_CO₂ – PRESENT_CO₂). Note the logarithmic color scale for present-day DIN and DFe concentrations (middle column).

to the comparatively small change in their growth rate (**Figure 6A**) and must have been caused by other factors. In comparison to the SP-SS + ST-SS (north) region, coccolithophore growth rates and biomass vary only little in the equatorial and the ST-SS (south) region (**Figure 6C and E**). As calcification is less inhibited by protons at preindustrial atmospheric CO₂, it can partly counteract the reduction in calcite concentrations caused by lower coccolithophore biomass in the SP-SS + ST-SS (north) region (**Figure 6A**). In the Southern Ocean, this disproportional effect of higher pH on calcification and on growth also explains why the difference in calcite concentration between present and preindustrial atmospheric CO₂ is stronger than in coccolithophore biomass (**Figure 6G**). Absolute differences in coccolithophore biomass and calcite, however, are negligible in this region due to the low initial concentrations, and changes in diatom and small-phytoplankton biomass are small (**Figure 6G**). Generally, differences in NPP follow differences in biomass, with slight discrepancies of up to 5% caused by changes in loss rates (**Figure 6A and E**). Altogether, small phytoplankton is most negatively and diatoms are most positively affected by preindustrial compared to present-day atmospheric CO₂ concentrations, while the global effects on coccolithophores and calcite are smaller and changes are confined to the regional scale.

3.2.2. Future versus present-day CO₂

Between future atmospheric CO₂ levels (750 μatm) and present-day CO₂ levels (420 μatm), globally averaged phytoplankton biomass and NPP change only marginally (less than 0.4%; **Table 4**). Except for slightly higher silicate exports at future atmospheric CO₂ concentrations (from 84 to 85.7 Tmol yr^{-1} ; **Table 4**), these marginal changes imply only a small CO₂ effect on globally averaged quantities.

In contrast to the global averages, CO₂ has pronounced regional and group-specific effects (**Figures 5 and 6B, D, F, and H**). On a regional scale, future coccolithophore growth rates are lower compared to present-day rates because of altered sensitivities to CO₂ and light, with up to 5% stronger limitations in both cases. Weakened nutrient limitation by up to 9%, primarily caused by DIN (**Figure 4D**) but also by DFe (**Figure 4E**), as well as the modulation of other factors (see Section *Unraveling the cascading effects of changing atmospheric CO₂ levels*) regionally compensates the growth-decreasing CO₂ and light effects (**Figure 6B, D, and F**). As a result, coccolithophore biomass is 12% and 14% higher (2% and 5% in the entire water column), respectively, in the equatorial and the SP-SS + ST-SS (north) region, and remains rather unchanged in the ST-SS (south) region. In all regions, the

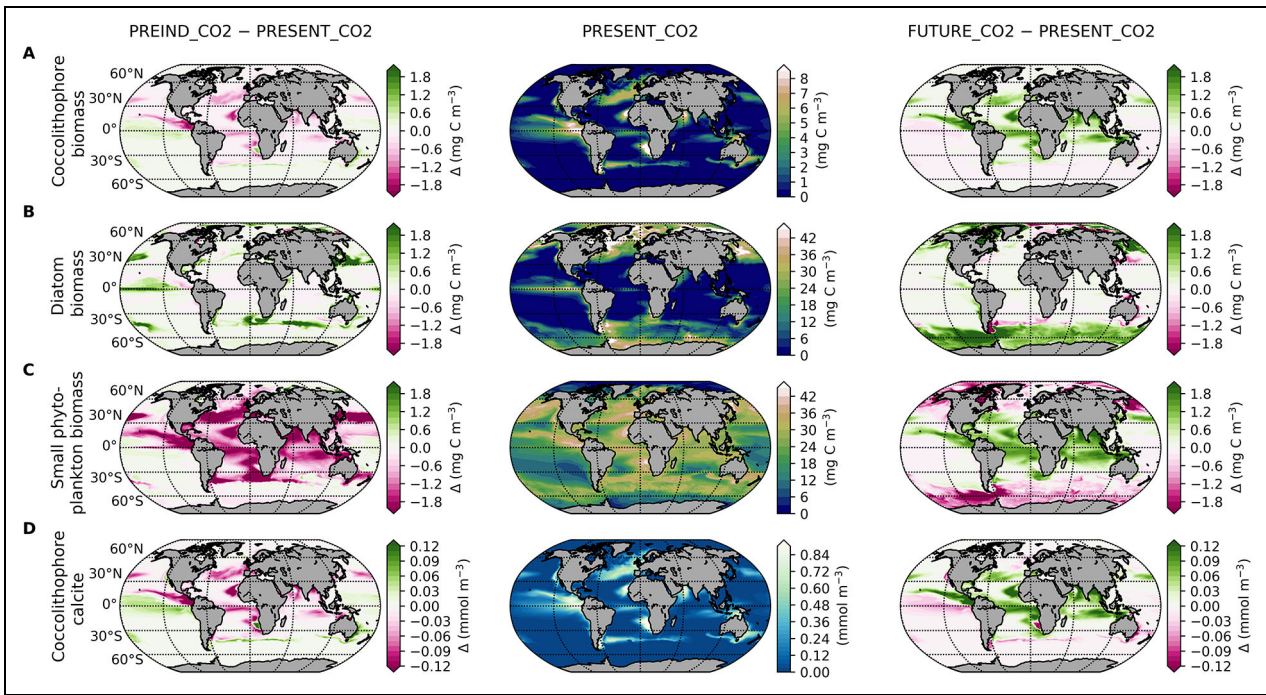


Figure 5. Surface phytoplankton biomass and coccolithophore calcite in model simulations. Maps display (A–C) surface phytoplankton biomass and (D) coccolithophore calcite concentration in the PRESENT_CO₂ simulation (middle column), and as total difference between the PRESENT_CO₂ simulation and the PREIND_CO₂ (left) and FUTURE_CO₂ (right) simulations, respectively (PREIND_CO₂ – PRESENT_CO₂ and FUTURE_CO₂ – PRESENT_CO₂).

negative impact of CO₂ on calcification increases by 8–10% (Figure 6B, D, and F). The biomass-related higher calcification and calcite concentrations are thereby dampened in the SP-SS + ST-SS (north) and equatorial regions, and both calcification and calcite concentrations are 8% lower in the ST-SS (south) region where coccolithophore biomass barely changes (Figure 6B, D, and F). Diatoms and small-phytoplankton biomass are barely affected by higher atmospheric CO₂ concentrations in the SP-SS + ST-SS (north), equatorial, and ST-SS (south) regions (Figure 6B, D, and F).

In the Southern Ocean (SP-SS + Ice (south) region), changes in CO_{2(aq)} and pH are strongest with 10–20% higher surface CO_{2(aq)} (up to 15–20 mmol m⁻³) and lower pH (up to 0.3 units; Figure 4A and C). Here, more growth-decreasing effects of CO₂ and light, partly counteracted by weakened nutrient limitation (Figure 4D and E), lower small-phytoplankton growth rates by about 3% and biomass by about 5% (Figure 6H). CO₂, light, and nutrient effects on diatoms and the resulting growth rate changes are less pronounced than for small phytoplankton, but have the same sign. Despite that similarity, diatom biomass increases by 8%, implying modulations of other factors (see Section *Unraveling the cascading effects of changing atmospheric CO₂ levels*). Relative changes in coccolithophore biomass and calcite in the Southern Ocean are negligible due to the generally low biomass and calcite concentrations.

As in the PREIND_CO₂ simulations, changes in NPP between the PRESENT_CO₂ and the FUTURE_CO₂ simulation follow changes in biomass, but vary slightly in magnitude with deviations up to 5% compared to biomass

differences (Figure 6B). In summary, the most pronounced changes compared to present-day CO₂ can be seen in the regionally higher coccolithophore biomass and its impact on calcite, as well as a shift to fewer diatoms and more small phytoplankton in the Southern Ocean at future atmospheric CO₂.

3.3. Unraveling the cascading effects of changing atmospheric CO₂ levels

We identify three cascading effects triggered by changes in atmospheric CO₂, which can modulate or even counteract the direct CO₂ effect on phytoplankton growth and biomass. CO₂ affects the nutrient and light limitation terms which feed back on the growth rate. The seasonal variation of the nutrient and light feedbacks determine the translation of direct CO₂ effects into biomass. Finally, we found an additional role of cascading effects via top-down factors. In the following, we explain each of the cascading effects for selected phytoplankton groups and regions (Figure 7A).

3.3.1. Nutrient and light feedbacks

Coccolithophore growth rates in the FUTURE_CO₂ simulation are strongly modified by alleviated nutrient limitation, stronger light limitation (Figure 6B, D, and F), and lower chlorophyll-to-carbon ratios (Figure S6) compared to the PRESENT_CO₂ simulation. Nutrient feedbacks are caused by a shift in the community structure and total biomass, leading to changes in available nutrients (Figure 7B). Light feedbacks are more complex (Figure 7C). Firstly, the nutrient limitation term f^N modifies the light limitation term f^L directly, with a stronger

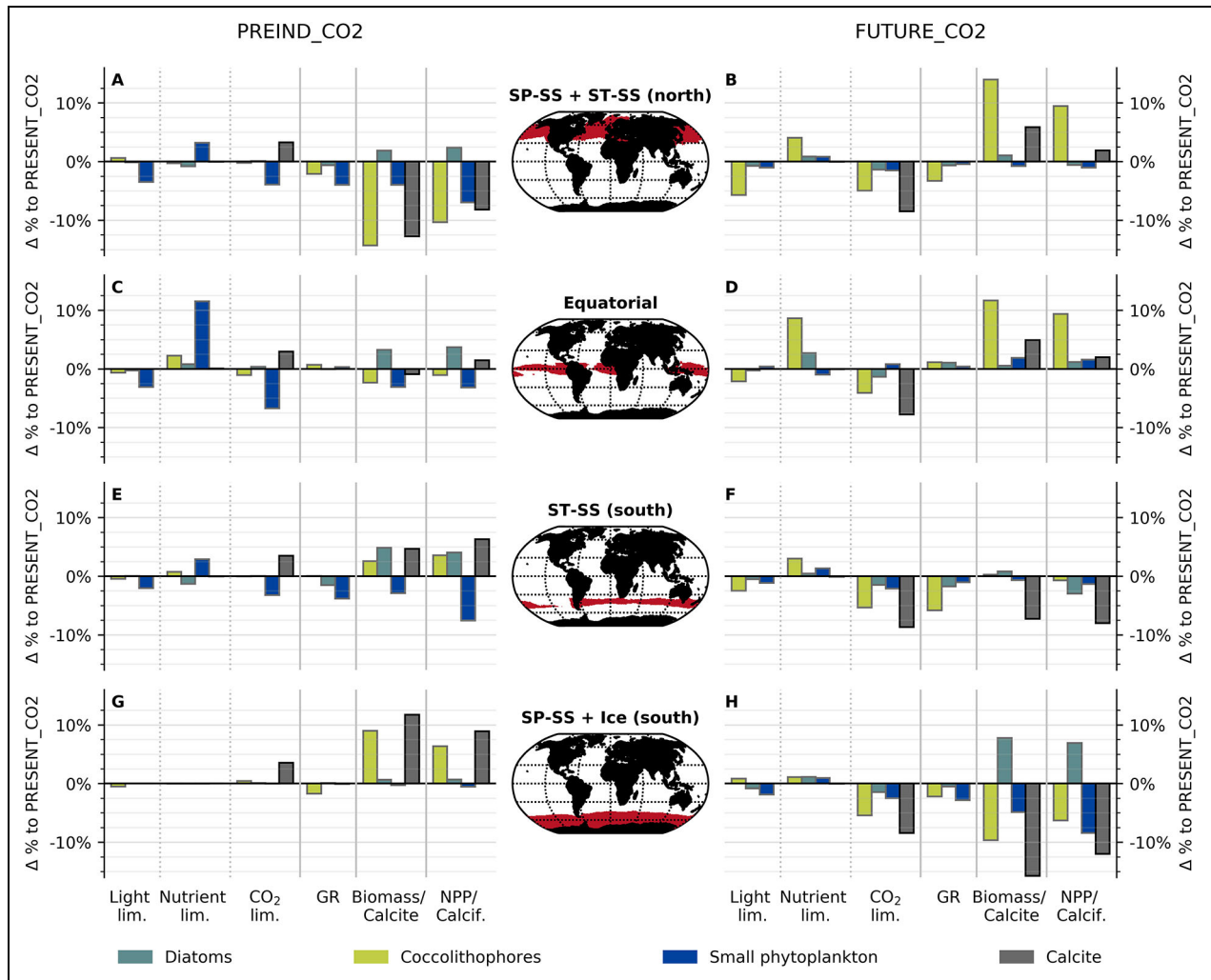


Figure 6. Variation in phytoplankton measures between preindustrial, present-day, and future simulations.

Barplots indicate relative changes in surface CO₂, light and nutrient limitation terms, phytoplankton growth rates, biomass, calcite concentrations, net primary production (NPP), and calcification between the PRESENT_CO2 simulation and the PREIND_CO2 (A, C, E, G) and FUTURE_CO2 (B, D, F, H) simulations, respectively, in four biomes denoted on the maps. Annual means for all parameters, spatial means for the limitation terms and growth rates, and spatial integrals for biomasses and NPP are presented. For calcification, we display the impact of nutrients and CO₂ on the (PIC:POC)_{cocco} ratio, as well as the change in integrated calcite mass; light is not affecting the (PIC:POC)_{cocco} ratio. A relative increase in a limitation term means that it is less limiting and therefore causes a higher growth rate and vice versa. SP = subpolar; ST = subtropic; SS = seasonal stratified; PS = permanently stratified, lim. = limitation; GR = growth rate; Calcif. = calcification.

light limitation under more replete nutrient conditions (Equation 5). Secondly, f^N modifies the chlorophyll-to-carbon ratio $q^{Chl:C}$ in f^L (Figure S6), because chlorophyll synthesis is dependent on biomass production of a phytoplankton group, but also varies with nitrogen assimilation and PAR (Hauck et al., 2013) which causes non-proportional changes in cellular chlorophyll and carbon concentrations. Phytoplankton can make less use of a prevailing light condition with a lower $q^{Chl:C}$. Finally, PAR has a direct impact on f^L , and is itself modified by the prevailing chlorophyll concentration in the watercolumn. Thus, lower nutrient limitation comes at the expense of stronger light limitation. Hence, the negative direct impact of high CO₂ levels on coccolithophores is modulated by these two feedbacks.

3.3.2. Seasonal variations of feedbacks

The nutrient and light feedbacks imposed by CO₂ dependencies vary seasonally, and manifest themselves most strongly in changes in biomass and NPP during the growing season (Figure 7B and C). For instance, while the negative effect of CO₂ and light on coccolithophore growth in the FUTURE_CO2 simulation can be counteracted partly by decreasing nutrient limitation in the annual mean, this effect cannot fully explain the considerably higher coccolithophore biomass in the SP-SS + ST-SS (north) region (Figure 6B). Monthly differences between the FUTURE_CO2 and the PRESENT_CO2 simulations show that coccolithophore growth rates are up to 5% higher between May and September at high atmospheric CO₂ (Figure 8A), caused by lower light and

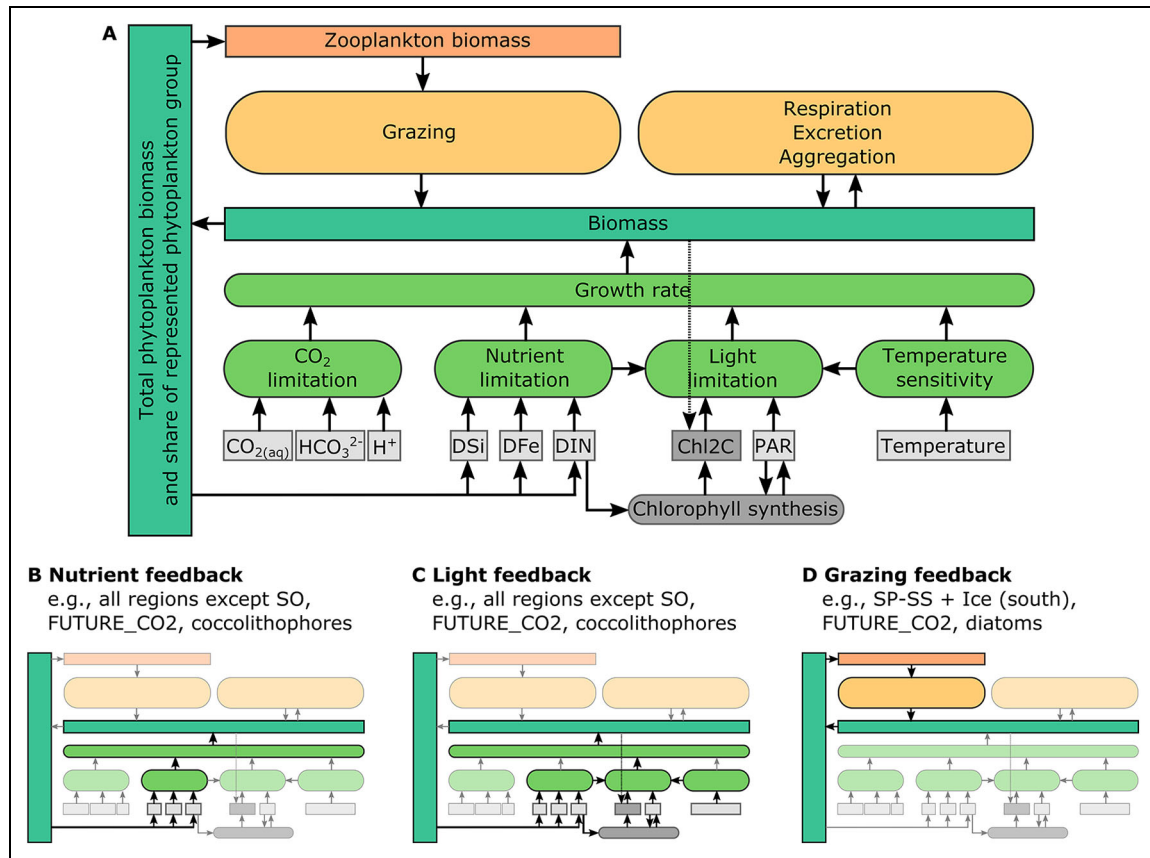


Figure 7. Cascading effects of environmental drivers and loss rates that affect the biomass of a single phytoplankton group in our model. (A) Overview of the processes affecting phytoplankton productivity and biomass. Besides direct impacts, modifications in CO₂ limitations can induce biomass changes through multiple feedback loops, i.e. via changes in nutrient and light limitation and in grazing. The temperature sensitivity remains unchanged at varying CO₂ levels. (B–D) Examples for nonlinear cascading CO₂ effects: (B and C) pathways of changes in nutrient and light limitations, respectively, for example, for future coccolithophores in all regions except from the Southern Ocean (SO); and (D) top-down effect by changes in the grazing pressure, for example, on future diatoms on the SP-SS + Ice (south) region.

nutrient limitation. As this period roughly coincides with the growing season with high initial biomass, it causes an annual mean increase in biomass and NPP. Lower annual mean growth rates at future compared to present-day CO₂ levels are caused by lower growth rates in winter (10–12% between October and April) due to a stronger light limitation and a relatively smaller alleviation in nutrient limitation compared to the remaining year, a time where initial biomass levels are low and changes in biomass and NPP are negligible. Annual means of growth rates are therefore often insufficient to explain changes in NPP and biomass, and the seasonality of cascading effects needs to be considered.

3.3.3. Grazing feedbacks

Finally, we identified modifications in the grazing pressure as another indirect CO₂ effect on phytoplankton biomass. Due to the variable grazing preference in our model (Fasam et al., 1990; Vallina et al., 2014), grazing fluxes change non-linearly with variations in the share of each phytoplankton group to total biomass as well as with changes in the total biomass of zooplankton (Figure 7D). Despite the higher diatom biomass in the

FUTURE_CO2 compared to the PRESENT_CO2 simulation (about 7%) due to increasing growth rates during summer in the SP-SS + Ice (south) region and the corresponding higher prey availability, grazing on diatoms decreases by about 6% in the respective months (Figure 8B). This decrease is caused by a lower zooplankton biomass, related to the decreasing small-phytoplankton biomass (Figure 6H), a food source that cannot be replaced entirely by diatoms (note grazing preferences in Section *Implementing coccolithophores into REcoM*). Lower grazing on diatoms in austral winter (June–August; Figure 8B) is a result of less diatom biomass. Grazing feedbacks also explain higher diatom biomass concentrations in the PRE-IND_CO2 simulation in all regions except from the Southern Ocean (Figure 6A, C, and E). Another example from the preindustrial SP-SS + ST-SS (north) region is the increasing grazing pressure on coccolithophores and their consequently lower biomass, which results from a combination of relatively high coccolithophore biomass in that region and biomass-decreasing effects of lower CO₂ on small phytoplankton which are then less available as prey. Other loss terms of phytoplankton biomass (respiration, excretion, aggregation) depend directly on the total

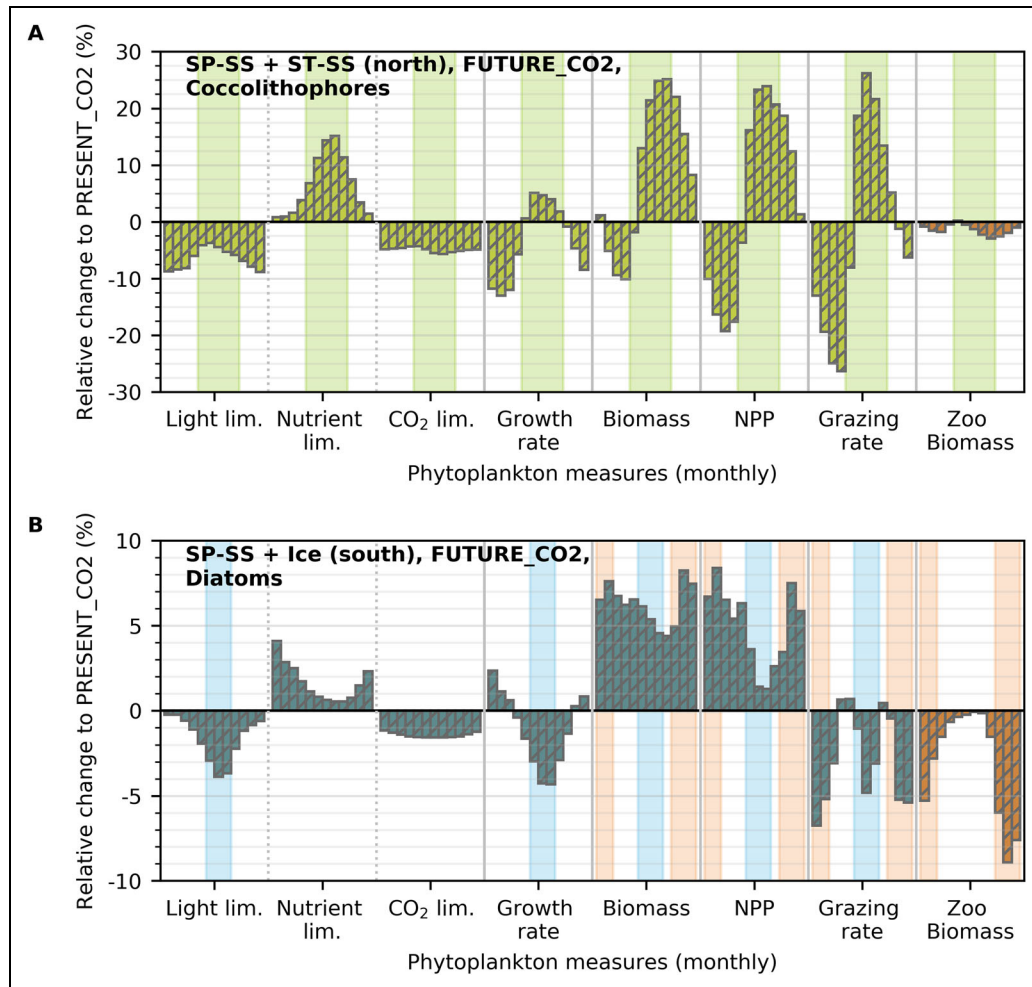


Figure 8. Simulated monthly variations in phytoplankton measures. Barplots indicate relative monthly changes (January–December) in surface light, nutrient and CO₂ limitation (lim.) terms, phytoplankton growth rates, biomasses, NPP, and grazing rates between the PRESENT_CO2 and the FUTURE_CO2 simulation for (A) coccolithophores in the SP-SS + ST-SS (north) region, and (B) diatoms in the SP-SS + Ice (south) region. Both panels also show the relative change in zooplankton (Zoo) biomass between the PRESENT_CO2 and the FUTURE_CO2 simulation (orange bars) in the respective region. Green shadings in (A) indicate the period of higher growth rates in the FUTURE_CO2 simulation compared to the PRESENT_CO2 simulation (May–September). Orange shadings in (B) indicate the months of decreasing grazing rate due to lower zooplankton biomass (October–February), and blue shadings indicate the months of decreasing grazing rate due to lower diatom productivity (June–August) in the FUTURE_CO2 simulation compared to the PRESENT_CO2 simulation.

phytoplankton and detritus biomass and/or biomass of the respective phytoplankton group and are not or negligibly affected by shifts in the share between phytoplankton groups. Hence, grazing on a phytoplankton group can be alleviated if the biomass of a zooplankton group decreases because its preferred prey is not present in sufficient abundance. In summary, cascading effects of CO₂ on light and nutrient limitations, on their seasonality, and on the grazing pressure are pivotal to the biomass and NPP responses of the phytoplankton groups.

3.4. Disentangling effects of historical warming and CO₂ increases on coccolithophore biomass changes

In our second set of simulations (Table 3) we aimed to disentangle the effects of warming and CO₂ on historical

changes in phytoplankton biomass. Globally, depth-integrated coccolithophore biomass levels in the VARCLI_VARCO2 simulation are highly variable in the simulated period (between 24 and 27 Tg C) with lower biomass in the 1990s–2000s compared to the 1960s–1970s (24–25 Tg C and 26–27 Tg C, respectively; Figure 9A). Over this time period, temperatures and CO_{2(aq)} concentrations increase by about 0.5°C and 0.003 mmol m⁻³, respectively (Figure 9B). Fluctuations in coccolithophore biomass levels are small at constant climatological forcing (CONSTCLI_VARCO2 simulation), implying that interannual variability of coccolithophore biomass is driven mainly by climate variability and, thus, combined alterations in temperature and CO_{2(aq)} concentrations. The lower CO_{2(aq)} concentration in the VARCLI_CONSTCO2 simulation compared to the VARCLI_VARCO2 simulation

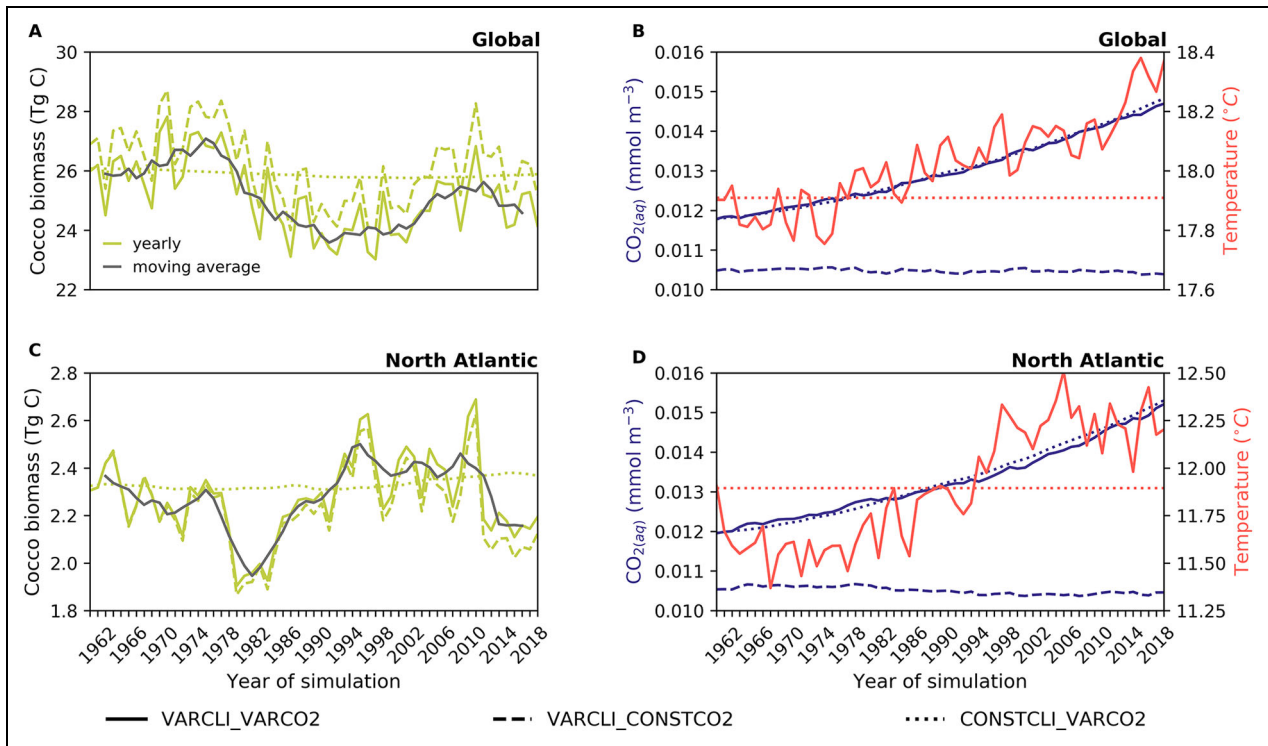


Figure 9. Time series of drift-corrected coccolithophore biomass, surface CO_{2(aq)} concentration, and surface temperature. Values are displayed (A and B) globally and (C and D) in the North Atlantic for the VARCLI_VARCO2 (solid line), VARCLI_CONSTCO2 (dashed line), and CONSTCLI_VARCO2 (dotted line) simulations (Table 3). Grey line (A and C) indicates the 5-year moving average of coccolithophore biomass in the VARCLI_VARCO2 simulation. Differences in CO_{2(aq)} (B and D) are caused mostly by different prescribed levels of atmospheric CO₂, and the effects of varying climate on CO_{2(aq)} are small (compare solid and dotted lines). Temperatures in the VARCLI_CONSTCO2 and the VARCLI_VARCO2 simulation are equal and therefore not distinguishable in panels B and D. Biomass concentrations were integrated over the entire water column. The first three years (1958–1960) were omitted in all simulations. For drift correction, the deviation between the control (CTRL) time-series and its initial value in 1961 was subtracted from the other simulations.

(−0.001 mmol m^{−3} at the beginning and increasing over the course of the time series) increases the coccolithophore biomass by almost 1 Tg C in the entire time period. However, increasing CO_{2(aq)} concentrations over time at constant temperature have almost no effect on the integrated coccolithophore biomass (CONSTCLI_VARCO2 simulation). Hence, according to our simulations, CO_{2(aq)} is not the main driver for global biomass changes since the 1960s, and variability in global coccolithophore biomass is driven mainly by climate variability.

In the North Atlantic, mean coccolithophore biomass levels in the 2000s are 4% higher than biomass levels in the 1960s (2.4 and 2.3 Tg C, respectively; Figure 9C). Our model therefore simulates a much smaller increase in coccolithophore biomass in the North Atlantic between 1960 and 2010 than the up to 10-fold increase in coccolithophore occurrence in observations (Beaugrand et al., 2013; Rivero-Calle et al., 2015; Krumhardt et al., 2016). After 2010, biomass levels decrease quickly by 0.2 Tg C, reaching biomass levels of 2.2 Tg C in 2019. Temperatures increase rapidly from about 11.5°C before the 1990s to about 12.25°C by the end of the time series with strong interannual variability, whereas CO_{2(aq)} concentrations increase steadily from about 12 × 10^{−3} mmol m^{−3} in the

1960s to about 15.5 × 10^{−3} mmol m^{−3} in the 2010s (Figure 9D). Thus, just as on a global scale, interannual biomass variability is caused by climate variability. In contrast to what is simulated on a global scale, however, biomass levels are increasingly higher over the course of the time series at increasing CO_{2(aq)} concentrations (VARCLI_VARCO2 simulation) than at constant CO_{2(aq)} concentrations (VARCLI_CONSTCO2 simulation, up to 0.1 Tg C in 2019; Figure 9C). This result is most likely due to a growth enhancing effect of higher CO_{2(aq)} concentrations, which are about 6 × 10^{−3} mmol m^{−3} higher in the VARCLI_VARCO2 compared to the VARCLI_CONSTCO2 simulation at the beginning of the time series, with increasing difference towards the end of the time series (Figure 9D). However, biomass levels barely change with increasing CO_{2(aq)} concentrations and constant temperature (CONSTCLI_VARCO2 simulation), pointing towards a small effect of CO_{2(aq)} on coccolithophore biomass in the period of the time series. We therefore attribute biomass changes predominantly to climate variability.

4. Discussion

Our model simulations show that adding a CO₂ dependence to phytoplankton growth leads to a cascade of

effects on (i) the growth rate of the individual phytoplankton groups by feedbacks on light and nutrient limitations and the seasonality therein (bottom-up effects), and (ii) the interaction between phytoplankton and zooplankton (top-down effects). In the *preindustrial global ocean*, small phytoplankton are affected most by direct and indirect CO₂ effects. The lower biomass of small phytoplankton in low to mid-latitudes causes lower zooplankton biomass concentrations and a shift of the grazing pressure to coccolithophores, which results regionally in up to 14% lower coccolithophore biomass. Diatoms, in contrast, benefit from lower zooplankton biomass rather than suffering from higher grazing pressure due to chosen grazing preferences, but effects are rather localized. In the *future global ocean*, coccolithophores are affected most by direct and indirect CO₂ effects, resulting in higher coccolithophore biomass. Changes in coccolithophore biomass affect the total phytoplankton biomass only marginally and therefore do not feed back on zooplankton biomass and grazing rates. In high latitudes, bottom-up effects cause lower small-phytoplankton biomass with consequently lower zooplankton biomass, which decreases the grazing pressure on diatoms. In low to mid-latitudes, bottom-up effects trigger slightly higher growth rates and biomass concentrations of small phytoplankton.

These results highlight two important aspects that shape top-down effects. Firstly, the standing stock of a group determines whether changes therein matter for the overall zooplankton prey availability (e.g., small phytoplankton versus coccolithophores). Secondly, the grazing preference determines if and how zooplankton can switch to a different prey (e.g., small phytoplankton and coccolithophores versus diatoms). The small zooplankton group in our model grazes preferentially on small phytoplankton and coccolithophores, and the polar macrozooplankton grazes mainly on diatoms. While the spatial distribution of polar macrozooplankton is confined to south of 50°S and north of 50°N, this group out-competes here the small zooplankton group due to its higher grazing efficiency. In the remaining ocean, grazing of the small-phytoplankton group dominates. A variety of grazing formulations are used in biogeochemical models which differ in how they describe prey switching and total grazing pressure, suggesting that using a different grazing parameterization can change the simulated grazing pressure on individual phytoplankton groups (Vallina et al., 2014). Nonetheless, given the good agreement of the simulated biomass fields in our simulations with observational data (Figures 3A and B and S4), we are confident that the qualitative dynamics of the feedbacks triggered by the addition of CO₂ dependencies also hold across grazing parameterizations. The complexity of modelled trophic interactions with partially unexpected feedbacks was also highlighted by Dutkiewicz et al. (2021), who showed that a small reduction in the abundance of one species can increase the total phytoplankton standing stock due to shifts to slower growing grazers and the freeing up of limiting nutrients, which is comparable to the cascading effects in our model. In the following, we discuss regional changes in phytoplankton biomass concentrations.

4.1. Cascading effects cause fewer small phytoplankton in the preindustrial ocean and more diatoms in the future Southern Ocean

In the preindustrial global ocean, small-phytoplankton biomass is lower compared to present-day CO₂ levels. Increasing levels of small-phytoplankton biomass over the last decades have also been shown in field and laboratory studies, with the projection of further increasing biomass with ongoing climate change (Daufresne et al., 2009; Peter and Sommer, 2012; Pinkerton et al., 2021). This beneficial effect has been associated with joint warming and increasing CO₂ (Hare et al., 2007; Feng et al., 2009). However, our model results suggest that even the carbonation effect alone, mainly caused by the large growth increase from preindustrial to present-day CO₂ levels, can lead to increasing biomass of small phytoplankton.

In the future Southern Ocean our model reveals a shift to less small phytoplankton and more diatom biomass compared to present-day CO₂ levels (Figures 5B and C and 6H). This advantage of diatoms over small phytoplankton is driven mainly by decreasing grazing pressure on diatoms (Figure 8B). In nature, the advantage of diatoms at future oceanic conditions may be further enhanced by alterations in the diatom species composition. Laboratory and mesocosm studies reveal that under ocean acidification, diatoms likely shift towards larger species (Tortell et al., 2008; Wu et al., 2014; Bach et al., 2019), changing community size structures and composition and having implications on the food web and biogeochemical cycling (Finkel et al., 2009; Alvarez-Fernandez et al., 2018). As currently we do not include cell size structure within a phytoplankton group in our model, accounting for shifts in this important trait (Dutkiewicz et al., 2015) could be a step forward to assess implications on export fluxes, with POC export likely increasing due to the higher biomass and ballasting of large diatom cells. While in parts of the Southern Ocean, a deepening of the mixed layer depth has been observed and modelled for recent years (Hauck et al., 2015; Panassa et al., 2018; Sallée et al., 2021) and future projections (Hauck et al., 2015), other regions may experience a temperature-driven stronger stratification (Constable et al., 2014). Small phytoplankton, because of their lower nutrient requirement, typically follow Southern Ocean diatom blooms that have drawn down nutrient concentrations (Irion et al., 2021). Similarly, a shoaling of the mixed layer would be more advantageous to small phytoplankton than for diatoms (Dutkiewicz et al., 2015; Petrou et al., 2016). Our results indicate, however, that increasing CO₂ levels may dampen the nutrient-driven advantage of small phytoplankton over diatoms in the future Southern Ocean (Figure 6H).

4.2. Alleviated nutrient limitation outbalances CO₂-induced decrease of coccolithophore growth in a high-CO₂ ocean

While laboratory CO₂ manipulation experiments tend to show either unaffected or decreasing coccolithophore growth rates between present-day and future CO₂ levels (e.g., Bach et al., 2013; Seifert et al., 2020; but see Meyer and Riebesell, 2015, for the diversity of responses),

coccolithophore biomass in our model is increasing due to the unexpected cascading effects that offset the negative effects of CO₂ on growth (**Figures 5A and 6B, D, and F**). Interactive effects between warming and high CO₂ conditions indicate a shift of the turning point between carbonation and acidification towards higher CO₂ levels at warmer temperatures (e.g., Sett et al., 2014; Gao et al., 2018), which may reduce the negative CO₂ effect on coccolithophores in the future scenario and ultimately lead to higher coccolithophore biomass, just as in our CO₂-only simulation. However, while the CO₂ limitation in our model showed only modest seasonal variations, mesocosm experiments have shown that a more severe CO₂-induced growth reduction at the beginning of the growing season can impede bloom formation and thereby reduce the overall ability to maintain sufficiently large seed populations for the ensuing growth seasons (Riebesell et al., 2017). Besides, a climate change-related increase in upper ocean stratification and the concomitant decrease in nutrient supply could increase the competitive fitness of small phytoplankton, as explained in Section *Cascading effects cause fewer small phytoplankton in the preindustrial ocean and more diatoms in the future Southern Ocean*, which could outweigh the negative effect of ocean acidification. Less nutrients are then available for diatoms and coccolithophores, which decreases their competitive fitness, an effect that cannot be seen in simulations where only atmospheric CO₂ is changed. Consequently, the negative CO₂ effect on coccolithophores could become more prevalent in a joint warming and high-CO₂ scenario, and decrease coccolithophore biomass in the future.

Our model suggests that the CO₂ impact on calcification, which is positive in the preindustrial and negative in the future ocean compared to present-day conditions, is modified and partly compensated by changes in coccolithophore biomass. Higher calcification rates under preindustrial CO₂ levels compared to the present-day in our study (**Figure 6C, E, and G**) seem to disagree with findings of Rigual-Hernández et al. (2020) who found that the thickness of the coccoliths barely differs between preindustrial samples, originating from sediment cores, and modern plankton samples. However, coccolith thickness and the sensitivity to CO₂ is highly species-specific (Rigual-Hernández et al., 2020), and shifts in coccolithophore species composition can impact patterns in calcite concentration and export (Beaufort et al., 2011). The number of coccoliths per cell is also variable, at least for *E. huxleyi*, and can additionally affect calcite concentrations under changing environmental conditions (Paasche, 2001). Whether or not there was a global trend towards lower calcification in all coccolithophore species from preindustrial to present-day remains unresolved.

In our simulations, calcification is the most sensitive process towards future CO₂ levels (**Figure 1**). Calcite concentrations increase in some regions (SP-SS + ST-SS (north and equatorial) only because of increasing coccolithophore biomass (**Figures 5A and 6B and D**). Based on the ballasting hypothesis (e.g., Klaas and Archer, 2002; Cram et al., 2018), this increase would be indicative of an increase of export production, which is currently not

represented in our model. Furthermore, while on a global scale, enhanced calcification and the accompanying CO₂ evolution affects the anthropogenic increase in atmospheric CO₂ only little (Gangstø et al., 2011), it can shape the regional air-sea CO₂ flux (Shutler et al., 2013).

4.3. Comparison to other modelling studies that include CO₂ dependencies

Increasing phytoplankton biomass and decreasing calcification at future CO₂ levels in our model compare well with the outcome of other modelling studies that include a CO₂ dependence of growth rates and/or calcification (Gangstø et al., 2011; Dutkiewicz et al., 2015; Krumhardt et al., 2019). Similar to our model, considerable alterations in global phytoplankton communities attributable to different sensitivities towards increasing CO₂ levels were simulated in the ecosystem model DARWIN of Dutkiewicz et al. (2015), whereas warming alone caused a poleward shift in phytoplankton dispersal with no significant impact on the community structure. While we used a mechanistic approach, Dutkiewicz et al. (2015) used a conceptual approach with a linear and positive dependence of growth rates on CO₂. They showed that decreasing nutrient availability due to stronger stratification lowers globally integrated primary production by 5% in 2100, which can be counteracted by CO₂-enhanced growth rates, leading to almost unchanged global primary production levels in 2100 compared to present-day levels. Similarly, Krumhardt et al. (2019) attributed global coccolithophore biomass increase to a direct CO₂ effect in their model. Contrary to these two studies which only account for the carbonation effect, we also modelled the acidification effect on phytoplankton growth whereby the direct CO₂ effect causes a decrease in future growth rates. However, cascading effects through nutrient and light feedbacks (**Figure 7**) can lead to an overall increase in biomass. While we did not simulate changes in circulation and stratification, we hypothesize that reduced nutrient availability in a more stratified ocean could reinforce rather than counteract the CO₂-driven decrease in growth. Thus, we rather expect a future decrease in phytoplankton biomass, which cannot be balanced by CO₂, different to the idealized simulations of Dutkiewicz et al. (2015).

In our model, increasing future coccolithophore biomass due to cascading effects over-compensates for the pH-driven decrease in calcification (**Figure 6B and D**), resulting in a net increase of global calcite concentrations that corresponds to the findings of Krumhardt et al. (2019). Both our study and that of Krumhardt et al. (2019) are in line with Gangstø et al. (2011), who projected a negative direct CO₂ effect on calcite production in a high emission scenario of the biogeochemical Bern3D/PISCES model. Going beyond the study of Gangstø et al. (2011) by modelling CO₂ effects on coccolithophore biomass, we have shown that biomass changes can compensate for decreasing calcite production, which is also in line with Krumhardt et al. (2019). In summary, our findings highlight the need to consider both carbonation and acidification effects on phytoplankton growth and coccolithophore calcification.

4.4. Increase in North Atlantic coccolithophore biomass is driven mainly by warming

According to our model, we attribute observed changes in North Atlantic coccolithophore biomass in recent decades primarily to warming and not to CO₂. Thus, our results largely comply with the warming hypothesis of Beaugrand et al. (2013), as changes in the modelled carbonate system during the 60 years of the time series are too small to have a pronounced effect on coccolithophore biomass. We thereby contrast the CO₂ hypotheses of Rivero-Calle et al. (2015) and Krumhardt et al. (2016), who concluded that warming alone did not control changes in coccolithophore biomass. Even with more significant shifts in the carbonate system, the negative impact of CO₂ on coccolithophore growth obtained by our model are overcompensated by more beneficial cascading effects on nutrient limitation (Section *Unraveling the cascading effects of changing atmospheric CO₂ levels*). Admittedly, none of the temperature functions in our model includes decreasing growth rates caused by temperature stress, which can considerably affect community structures (e.g., D'Amario et al., 2020), but we suppose that thermally stressed species or ecotypes would be replaced by more heat-tolerant species or ecotypes of the same phytoplankton group, resulting in the same changes in coccolithophore biomass as simulated here. We expect thermal stress to become more relevant in polar regions and/or for a more intense temperature increase that outpaces the speed of species migration, but not for the given temperature increase within 60 years in the North Atlantic. We additionally need to bear in mind that our parameterization aims to represent the diverse group of coccolithophores, while the North Atlantic coccolithophore community is dominated by the fast growing, bloom-forming *E. huxleyi* (Haidar and Thierstein, 2001; Balch et al., 2019), which may respond more strongly to changing CO₂ conditions than coccolithophores in our model. Besides, the CO₂ effect on coccolithophore growth would be different if extreme CO₂ levels of laboratory experiments had been excluded from the parameterization. Based on our model results, however, we conclude that the direct CO₂ impact on coccolithophore biomass in the recent decades, globally and in the North Atlantic, is small compared to the effect of warming, supporting the hypothesis of Beaugrand et al. (2013).

4.5. Limitations and caveats

Our description of CO₂ dependencies goes well beyond previous studies by developing mechanistic response functions of phytoplankton functional type growth rates and coccolithophore calcification. We are confident that it captures the first-order effects of CO₂ on phytoplankton biomass and NPP. Nevertheless, we acknowledge that additional processes (i.e., multiple driver interactions, mixotrophy, CO₂ effects on silicification and zooplankton, adaptation and evolution, as well as mesozooplankton grazing) have the potential to further modify the response of the marine ecosystem to high-CO₂ levels in simulations and in the real world.

The response of phytoplankton growth and calcification to changing CO₂ levels can be modified significantly by synergistic and antagonistic interactions with other environmental drivers such as temperature and light (e.g., Harvey et al., 2013; Brandenburg et al., 2019; Seifert et al., 2020), and can result in enhanced or dampened responses than expected from CO₂ alone. However, most biogeochemical models, including ours, do not account for the interaction between environmental drivers. For instance, acidification affects the response to nutrient availability of coccolithophores (Zondervan, 2007; Zhang et al., 2019) and other phytoplankton groups (Li et al., 2012; Spungin et al., 2014; Li et al., 2017). The beneficial effect of nutrients on coccolithophore biomass in the FUTURE_CO2 simulation may thus be weakened by acidification, and therefore dampen the biomass increase compared to present-day conditions. The implementation of multiple driver interactions would therefore be a crucial amendment to phytoplankton modelling.

Mixotrophy, which is the capacity of an organism to live auto- and heterotrophically, can reduce the vulnerability of phytoplankton to environmental changes, for example, under substrate limitation (low carbonation) of photosynthesis. Mixotrophy is very common in species that we summarize as small phytoplankton (Stoecker et al., 2017), but some coccolithophore species can live mixotrophically as well (Godrijan et al., 2020). While our phytoplankton growth rate parameterization is based entirely on photosynthesis, effects of changing CO₂ levels could be diminished if we additionally considered the possibility to switch to mixotrophy when CO₂ or other conditions become unfavorable. Besides, not only calcification, but also silicification by diatoms appears to be CO₂ sensitive (Petrou et al., 2019). Although this sensitivity could alter the response of diatoms towards increasing CO₂ conditions and, for instance, possibly hamper the success of diatoms in the future Southern Ocean, the knowledge about this relationship is still too limited to be incorporated into modelling approaches. Similarly, CO₂ effects on grazers and higher trophic levels could further modify the ecosystem response (Cripps et al., 2014).

Adaptation and evolution can shape substantially the response of phytoplankton towards high or low *p*CO₂ levels (Brennan et al., 2017), processes that are not usually considered in ocean biogeochemical models. For instance, coccolithophores can adapt within months or years to warming and high CO₂ conditions (Schlüter et al., 2014). However, with the current pace of environmental changes caused by climate change and the limits of adaptation, whether adaptational and evolutionary processes are fast enough to offset negative effects of environmental driver changes is questionable. The assessment of abilities and speed of phytoplankton (and other organism) adaptations is challenging (Kelly and Griffiths, 2021), and the data basis remains highly varied among studies, which currently prevents a robust implementation into biogeochemical models.

While our model represents a polar macrozooplankton as well as a generic small zooplankton group, it does not include mesozooplankton, which is globally distributed

(Moriarty and O'Brien, 2013) and an important component of trophic interactions and the biological carbon pump (Buitenhuis et al., 2006). Hence, considering mesozooplankton could alter the grazing feedbacks presented in our study, for instance in the Southern Ocean where the grazing pressure on diatoms is indirectly lowered due to the decrease of small-phytoplankton biomass.

4.6. Conclusions

Model projections are the primary tool to understand future shifts in marine productivity and its impact on higher trophic levels and food webs. Even if the resilience of phytoplankton communities to climate change-related impacts might be relatively high because environmental niches can be re-occupied by species that are better adapted to the new environmental conditions (Dutkiewicz et al., 2021), most models project a future decrease in global NPP, with a large spread in the magnitude across different models (Kwiatkowski et al., 2020). Carbonation and acidification may have a relatively smaller effect on phytoplankton growth than other environmental drivers such as warming or changes in nutrient availability, but these processes will become increasingly important with ongoing ocean acidification. Our study highlights that CO₂, especially due to its cascading effects on light and nutrient limitation and grazing, can change regional phytoplankton community compositions and primary production considerably in a simulation with future atmospheric CO₂ concentrations. Modifications in biomass concentrations can locally account for 10% and more. In addition, other studies reveal that CO₂ can tip the scale when multiple driver interactions are involved (e.g., Harvey et al., 2013; Brandenburg et al., 2019; Seifert et al., 2020). Accounting for carbonation and acidification effects on phytoplankton growth and calcification in model projections adds an important physiological constraint on primary production and biogeochemical cycling in the future ocean.

Data accessibility statement

Model data necessary to produce the findings of this study are archived in Zenodo (<https://zenodo.org/>; Seifert and Hauck, 2022). Full model output can be requested from the corresponding author.

Supplemental files

The supplemental files for this article can be found as follows:

Figures S1–S6.pdf
Text S1.pdf
Tables S1–S4.pdf

Acknowledgments

We thank Meike Vogt from ETH Zurich, Switzerland, and Colleen O'Brien for providing gridded data products of coccolithophore biomass concentrations for our model evaluation. Furthermore, we thank Frédéric Maps and an anonymous reviewer for their constructive comments and suggestions.

Funding

This research was supported under the Initiative and Networking Fund of the Helmholtz Association (Helmholtz Young Investigator Group Marine Carbon and Ecosystem Feedbacks in the Earth System [MarESys], grant number VH-NG-1301) as well as the European Union's Horizon 2020 research and innovation program under grant agreement number 869357 (project OceanNETs: Ocean-based Negative Emission Technologies—analyzing the feasibility, risks, and co-benefits of ocean-based negative emission technologies for stabilizing the climate). MS acknowledges funding from the Helmholtz Graduate School for Polar and Marine Research POLMAR. CN has received funding from the European Union's Horizon 2020 research and innovation program under grant agreement number 820989 (project COMFORT). The work reflects only the authors' views; the European Commission and their executive agency are not responsible for any use that may be made of the information the work contains.

Competing interests

The authors have no competing interests, as defined by Elementa, that might be perceived to influence the research presented in this article.

Author contributions

Contributed to conception and design: MS, CN, BR, JH.

Contributed to acquisition of data: MS, CN, BR, JH.

Contributed to analysis and interpretation of data: MS, CN, BR, JH.

Drafted and/or revised the article: MS, CN, BR, JH.

Approved the submitted version for publication: MS, CN, BR, JH.

References

- Alvarez-Fernandez, S, Bach, LT, Taucher, J, Riebesell, U, Sommer, U, Aberle, N, Brussaard, CPD, Boersma, M.** 2018. Plankton responses to ocean acidification: The role of nutrient limitation. *Progress in Oceanography* **165**: 11–18. DOI: <https://dx.doi.org/10.1016/j.pocean.2018.04.006>.
- Aumont, O, Ethé, C, Tagliabue, A, Bopp, L, Gehlen, M.** 2015. PISCES-v2: An ocean biogeochemical model for carbon and ecosystem studies. *Geoscientific Model Development* **8**(8): 2465–2513. DOI: <http://dx.doi.org/10.5194/gmd-8-2465-2015>.
- Aumont, O, Maier-Reimer, E, Blain, S, Monfray, P.** 2003. An ecosystem model of the global ocean including Fe, Si, P colimitations. *Global Biogeochemical Cycles* **17**(2): 1–26. DOI: <http://dx.doi.org/10.1029/2001GB001745>.
- Bach, LT.** 2015. Reconsidering the role of carbonate ion concentration in calcification by marine organisms. *Biogeosciences* **12**(16): 4939–4951. DOI: <http://dx.doi.org/10.5194/bg-12-4939-2015>.
- Bach, LT, Hernández-Hernández, N, Taucher, J, Spisla, C, Sforza, C, Riebesell, U, Arístegui, J.** 2019. Effects of elevated CO₂ on a natural diatom community in the subtropical NE Atlantic. *Frontiers in*

- Marine Science* **6**: 75. DOI: <http://dx.doi.org/10.3389/fmars.2019.00075>.
- Bach, LT, Mackinder, LCM, Schulz, KG, Wheeler, G, Schroeder, DC, Brownlee, C, Riebesell, U.** 2013. Dissecting the impact of CO₂ and pH on the mechanisms of photosynthesis and calcification in the coccolithophore *Emiliania huxleyi*. *New Phytologist* **199**(1): 121–134. DOI: <http://dx.doi.org/10.1111/nph.12225>.
- Bach, LT, Riebesell, U, Gutowska, MA, Federwisch, L, Schulz, KG.** 2015. A unifying concept of coccolithophore sensitivity to changing carbonate chemistry embedded in an ecological framework. *Progress in Oceanography* **135**: 125–138. DOI: <http://dx.doi.org/10.1016/j.pocean.2015.04.012>.
- Bach, LT, Riebesell, U, Schulz, KG.** 2011. Distinguishing between the effects of ocean acidification and ocean carbonation in the coccolithophore *Emiliania huxleyi*. *Limnology and Oceanography* **56**(6): 2040–2050. DOI: <http://dx.doi.org/10.4319/lo.2011.56.6.2040>.
- Balch, WM, Bowler, BC, Drapeau, DT, Lubelczyk, LC, Lyczkowski, E, Mitchell, C, Wyeth, A.** 2019. Coccolithophore distributions of the North and South Atlantic Ocean. *Deep Sea Research Part I: Oceanographic Research Papers* **151**: 103066. DOI: <http://dx.doi.org/10.1016/j.dsr.2019.06.012>.
- Balch, WM, Drapeau, DT, Bowler, BC, Lyczkowski, E, Booth, ES, Alley, D.** 2011. The contribution of coccolithophores to the optical and inorganic carbon budgets during the Southern Ocean Gas Exchange Experiment: New evidence in support of the “Great Calcite Belt” hypothesis. *Journal of Geophysical Research: Oceans* **116**(C4): 1–14. DOI: <http://dx.doi.org/10.1029/2011JC006941>.
- Barcelos e Ramos, J, Schulz, KG, Brownlee, C, Sett, S, Azevedo, EB.** 2014. Effects of increasing seawater carbon dioxide concentrations on chain formation of the diatom *Asterionellopsis glacialis*. *PLoS One* **9**(3): 1–8. DOI: <http://dx.doi.org/10.1371/journal.pone.0090749>.
- Barrett, PM, Resing, JA, Buck, NJ, Feely, RA, Bullister, JL, Buck, CS, Landing, WM.** 2014. Calcium carbonate dissolution in the upper 1000 m of the eastern North Atlantic. *Global Biogeochemical Cycles* **28**(4): 386–397. DOI: <http://dx.doi.org/10.1002/2013GB004619>.
- Barton, AD, Irwin, AJ, Finkel, ZV, Stock, CA.** 2016. Anthropogenic climate change drives shift and shuffle in North Atlantic phytoplankton communities. *Proceedings of the National Academy of Sciences* **113**(11): 2964–2969. DOI: <http://dx.doi.org/10.1073/pnas.1519080113>.
- Battaglia, G, Steinacher, M, Joos, F.** 2016. A probabilistic assessment of calcium carbonate export and dissolution in the modern ocean. *Biogeosciences* **13**(9): 2823–2848. DOI: <http://dx.doi.org/10.5194/bg-13-2823-2016>.
- Beardall, J, Raven, JA.** 2013. Calcification and ocean acidification: New insights from the coccolithophore *Emiliania huxleyi*. *New Phytologist* **199**(1): 1–3. DOI: <http://dx.doi.org/10.1111/nph.12297>.
- Beaufort, L, Probert, I, de Garidel-Thoron, T, Bendif, EM, Ruiz-Pino, D, Metzl, N, Goyet, C, Buchet, N, Coupel, P, Grelaud, M, Rost, B, Rickaby, REM, de Vargas, C.** 2011. Sensitivity of coccolithophores to carbonate chemistry and ocean acidification. *Nature* **476**(7358): 80–83. DOI: <http://dx.doi.org/10.1038/nature10295>.
- Beaugrand, G, McQuatters-Gollop, A, Edwards, M, Goberville, E.** 2013. Long-term responses of North Atlantic calcifying plankton to climate change. *Nature Climate Change* **3**(3): 263–267. DOI: <http://dx.doi.org/10.1038/nclimate1753>.
- Behrenfeld, MJ, Falkowski, PG.** 1997. Photosynthetic rates derived from satellite-based chlorophyll concentration. *Limnology and Oceanography* **42**(1): 1–20. DOI: <http://dx.doi.org/10.4319/lo.1997.42.1.0001>.
- Berelson, WM, Balch, WM, Najjar, R, Feely, RA, Sabine, C, Lee, K.** 2007. Relating estimates of CaCO₃ production, export, and dissolution in the water column to measurements of CaCO₃ rain into sediment traps and dissolution on the sea floor: A revised global carbonate budget. *Global Biogeochemical Cycles* **21**(1): 1–15. DOI: <http://dx.doi.org/10.1029/2006GB002803>.
- Bindoff, NL, Cheung, WWL, Kairo, JG, Arístegui, J, Guinder, VA, Hallberg, R, Hilmi, N, Jiao, N, Karim, NS, Levin, L, O’Donoghue, S, Purca Cuicapusa, SR, Rinkevich, B, Suga, T, Tagliabue, A, Williamson, P.** 2019. Changing ocean, marine ecosystems, and dependent communities, in Pörtner, HO, Roberts, DC, Masson-Delmotte, V, Zhai, P, Tignor, M, Poloczanska, E, Mintenbeck, K, Alegria, A, Nicolai, M, Okem, A, Petzold, J, Rama, B, Weyer, NM eds., *IPCC special report on the ocean and cryosphere in a changing climate*. New York, NY: Cambridge University Press: 447–587. DOI: <http://dx.doi.org/10.1017/9781009157964.007>.
- Boatman, TG, Davey, PA, Lawson, T, Geider, RJ.** 2018. CO₂ modulation of the rates of photosynthesis and light-dependent O₂ consumption in *Trichodesmium*. *Journal of Experimental Botany* **70**(2): 589–597. DOI: <http://dx.doi.org/10.1093/jxb/ery368>.
- Boye, M, van den Berg, CMG, de Jong, JTM, Leach, H, Croot, P, de Baar, HJW.** 2001. Organic complexation of iron in the Southern Ocean. *Deep Sea Research Part I: Oceanographic Research Papers* **48**(6): 1477–1497. DOI: [http://dx.doi.org/10.1016/S0967-0637\(00\)00099-6](http://dx.doi.org/10.1016/S0967-0637(00)00099-6).
- Brandenburg, KM, Velthuis, M, Van de Waal, DB.** 2019. Meta-analysis reveals enhanced growth of marine harmful algae from temperate regions with warming and elevated CO₂ levels. *Global Change Biology* **25**: 2607–2618. DOI: <http://dx.doi.org/10.1111/gcb.14678>.
- Brennan, GL, Colegrave, N, Collins, S.** 2017. Evolutionary consequences of multidriver environmental change in an aquatic primary producer. *Proceedings*

- of the National Academy of Sciences **114**(37): 9930–9935. DOI: <http://dx.doi.org/10.1073/pnas.1703375114>.
- Brownlee, C, Taylor, A.** 2004. Chapter, Calcification in coccolithophores: A cellular perspective, in Thierstein, HR, Young, JR eds., *Coccolithophores*. Berlin, Germany: Springer. DOI: http://dx.doi.org/10.1007/978-3-662-06278-4_2.
- Buitenhuis, ET, Hashioka, T, Quéré, CL.** 2013. Combined constraints on global ocean primary production using observations and models. *Global Biogeochemical Cycles* **27**(3): 847–858. DOI: <http://dx.doi.org/10.1002/gbc.20074>.
- Buitenhuis, ET, Le Quéré, C, Aumont, O, Beaugrand, G, Bunker, A, Hirst, A, Ikeda, T, O'Brien, T, Piontkovski, S, Straile, D.** 2006. Biogeochemical fluxes through mesozooplankton. *Global Biogeochemical Cycles* **20**(2): 1–18. DOI: <http://dx.doi.org/10.1029/2005GB002511>.
- Buitenhuis, ET, Vogt, M, Moriarty, R, Bednaršek, N, Doney, SC, Leblanc, K, Le Quéré, C, Luo, YW, O'Brien, C, O'Brien, T, Peloquin, J, Schiebel R, Swan, C.** 2013. MAREDAT: Towards a world atlas of MARine Ecosystem DATa. *Earth System Science Data* **5**(2): 227–239. DOI: <http://dx.doi.org/10.5194/essd-5-227-2013>.
- Carr, ME, Friedrichs, MA, Schmeltz, M, Noguchi Aita, M, Antoine, D, Arrigo, KR, Asanuma, I, Aumont, O, Barber, R, Behrenfeld, M, Bidigare, R, Buitenhuis, ET, Campbell, J, Ciotti, A, Dierssen, H, Dowell, M, Dunne, J, Esaias, W, Gentili, B, Gregg, W, Groom, S, Hoepffner, N, Ishizaka, J, Kameda, T, Quéré, CL, Lohrenz, S, Marra, J, Mélin, F, Moore, K, Morel, A, Reddy, TE, Ryan, J, Scardi, M, Smyth, T, Turpie, K, Tilstone, G, Waters, K, Yamanaka, Y.** 2006. A comparison of global estimates of marine primary production from ocean color. *Deep Sea Research Part II: Topical Studies in Oceanography* **53**(5): 741–770. DOI: <http://dx.doi.org/10.1016/j.dsr2.2006.01.028>.
- Constable, AJ, Melbourne-Thomas, J, Corney, SP, Arrigo, KR, Barbraud, C, Barnes, DKA, Bindoff, NL, Boyd, PW, Brandt, A, Costa, DP, Davidson, AT, Ducklow, HW, Emmerson, L, Fukuchi, M, Gutt, J, Hindell, MA, Hofmann, EE, Hosie, GW, Iida, T, Jacob, S, Johnston, NM, Kawaguchi, S, Kokubun, N, Koubbi, P, Lea, M-A, Makhado, A, Massom, RA, Meiners, K, Meredith, MP, Murphy, EJ, Nicol, S, Reid, K, Richerson, K, Riddle, MJ, Rintoul, SR, Smith, WO Jr, Southwell, C, Stark, JS, Sumner, M, Swadling, KM, Takahashi, KT, Trathan, PN, Welsford, DC, Weimerskirch, H, Westwood, KJ, Wienecke, BC, Wolf-Gladrow, D, Wright, SW, Xavier, JC, Ziegler, P.** 2014. Climate change and Southern Ocean ecosystems I: How changes in physical habitats directly affect marine biota. *Global Change Biology* **20**(10): 3004–3025. DOI: <http://dx.doi.org/10.1111/gcb.12623>.
- Cram, JA, Weber, T, Leung, SW, McDonnell, AMP, Liang, JH, Deutsch, C.** 2018. The role of particle size, ballast, temperature, and oxygen in the sinking flux to the deep sea. *Global Biogeochemical Cycles* **32**(5): 858–876. DOI: <http://dx.doi.org/10.1029/2017GB005710>.
- Cripps, G, Lindeque, P, Flynn, KJ.** 2014. Have we been underestimating the effects of ocean acidification in zooplankton? *Global Change Biology* **20**(11): 3377–3385. DOI: <http://dx.doi.org/10.1111/gcb.12582>.
- D'Amario, B, Pérez, C, Grelaud, M, Pitta, P, Krasakopoulou, E, Ziveri, P.** 2020. Coccolithophore community response to ocean acidification and warming in the Eastern Mediterranean Sea: Results from a mesocosm experiment. *Scientific Reports* **10**(1): 1–14. DOI: <http://dx.doi.org/10.1038/s41598-020-69519-5>.
- Daufresne, M, Lengfellner, K, Sommer, U.** 2009. Global warming benefits the small in aquatic ecosystems. *Proceedings of the National Academy of Sciences* **106**(31): 12788–12793. DOI: <http://dx.doi.org/10.1073/pnas.0902080106>.
- de Baar, HJW, de Jong, JTM, Nolting, RF, Timmermans, KR, van Leeuwe, MA, Bathmann, U, Rutgers van der Loeff, M, Sildam, J.** 1999. Low dissolved Fe and the absence of diatom blooms in remote Pacific waters of the Southern Ocean. *Marine Chemistry* **66**(1): 1–34. DOI: [http://dx.doi.org/10.1016/S0304-4203\(99\)00022-5](http://dx.doi.org/10.1016/S0304-4203(99)00022-5).
- Doney, SC, Fabry, VJ, Feely, RA, Kleypas, JA.** 2009. Ocean acidification: The other CO₂ problem. *Annual Review of Marine Science* **1**(1): 169–192. DOI: <http://dx.doi.org/10.1146/annurev.marine.010908.163834>.
- Dunne, JP, Sarmiento, JL, Gnanadesikan, A.** 2007. A synthesis of global particle export from the surface ocean and cycling through the ocean interior and on the seafloor. *Global Biogeochemical Cycles* **21**(4): 1–16. DOI: <http://dx.doi.org/10.1029/2006GB002907>.
- Dutkiewicz, S, Boyd, PW, Riebesell, U.** 2021. Exploring biogeochemical and ecological redundancy in phytoplankton communities in the global ocean. *Global Change Biology* **27**(6): 1196–1213. DOI: <http://dx.doi.org/10.1111/gcb.15493>.
- Dutkiewicz, S, Morris, JJ, Follows, MJ, Scott, J, Levitan, O, Dyhrman, ST, Berman-Frank, I.** 2015. Impact of ocean acidification on the structure of future phytoplankton communities. *Nature Climate Change* **5**(11): 1002–1006. DOI: <http://dx.doi.org/10.1038/NCLIMATE2722>.
- Eichner, M, Kranz, SA, Rost, B.** 2014. Combined effects of different CO₂ levels and N sources on the diazotrophic cyanobacterium. *Trichodesmium. Physiologia Plantarum* **152**(2): 316–330. DOI: <http://dx.doi.org/10.1111/ppl.12172>.
- Eyring, V, Bony, S, Meehl, GA, Senior, CA, Stevens, B, Stouffer, RJ, Taylor, KE.** 2016. Overview of the Coupled Model Intercomparison Project Phase 6 (CMIP6) experimental design and organization.

- Geoscientific Model Development* **9**(5): 1937–1958. DOI: <http://dx.doi.org/10.5194/gmd-9-1937-2016>.
- Fasham, MJR, Ducklow, HW, McKelvie, SM.** 1990. A nitrogen-based model of plankton dynamics in the oceanic mixed layer. *Journal of Marine Research* **48**(3): 591–639. DOI: <http://dx.doi.org/10.1357/002224090784984678>.
- Fay, AR, McKinley, GA.** 2014. Global open-ocean biomes: Mean and temporal variability. *Earth System Science Data* **6**(2): 273–284. DOI: <http://dx.doi.org/10.5194/essd-6-273-2014>.
- Feely, RA, Sabine, CL, Lee, K, Berelson, W, Kleypas, J, Fabry, VJ, Millero, FJ.** 2004. Impact of anthropogenic CO₂ on the CaCO₃ system in the oceans. *Science* **305**(5682): 362–366. DOI: <http://dx.doi.org/10.1126/science.1097329>.
- Feng, Y, Hare, CE, Leblanc, K, Rose, JM, Zhang, Y, DiTullio, GR, Lee, PA, Wilhelm, SW, Rowe, JM, Sun, J, Nemcek, N, Gueguen, C, Passow, U, Benner, I, Brown, C, Hutchins, DA.** 2009. Effects of increased pCO₂ and temperature on the North Atlantic spring bloom. I. The phytoplankton community and biogeochemical response. *Marine Ecology Progress Series* **388**: 13–25. DOI: <http://dx.doi.org/10.3354/meps08133>.
- Feng, Y, Roleda, MY, Armstrong, E, Boyd, PW, Hurd, CL.** 2017. Environmental controls on the growth, photosynthetic and calcification rates of a Southern Hemisphere strain of the coccolithophore. *Emiliania huxleyi*. *Limnology and Oceanography* **62**(2): 519–540. DOI: <http://dx.doi.org/10.1002/lno.10442>.
- Field, CB, Behrenfeld, MJ, Randerson, JT, Falkowski, P.** 1998. Primary production of the biosphere: Integrating terrestrial and oceanic components. *Science* **281**(5374): 237–240. DOI: <http://dx.doi.org/10.1126/science.281.5374.237>.
- Fielding, SR.** 2013. *Emiliania huxleyi* specific growth rate dependence on temperature. *Limnology and Oceanography* **58**(2): 663–666. DOI: <http://dx.doi.org/10.4319/lo.2013.58.2.0663>.
- Findlay, HS, Calosi, P, Crawford, K.** 2011. Determinants of the PIC:POC response in the coccolithophore *Emiliania huxleyi* under future ocean acidification scenarios. *Limnology and Oceanography* **56**(3): 1168–1178. DOI: <http://dx.doi.org/10.4319/lo.2011.56.3.1168>.
- Finkel, ZV, Beardall, J, Flynn, KJ, Quigg, A, Rees, TAV, Raven, JA.** 2009. Phytoplankton in a changing world: Cell size and elemental stoichiometry. *Journal of Plankton Research* **32**(1): 119–137. DOI: <http://dx.doi.org/10.1093/plankt/fbp098>.
- Follows, MJ, Dutkiewicz, S, Grant, S, Chisholm, SW.** 2007. Emergent biogeography of microbial communities in a model ocean. *Science* **315**(5820): 1843–1846. DOI: <http://dx.doi.org/10.1126/science.1138544>.
- Friedlingstein, P, O'Sullivan, M, Jones, MW, Andrew, RM, Hauck, J, Olsen, A, Peters, GP, Peters, W, Pongratz, J, Sitch, S, Quéré, CL, Canadell, JG, Ciais, P, Jackson, RB, Alin, S, Aragão, LEOC, Arneeth, A, Arora, V, Bates, NR, Becker, M, Benoit-Cattin, A, Bittig, HC, Bopp, L, Bultan, S, Chandra, N, Chevallier, F, Chini, LP, Evans, W, Florentie, L, Forster, PM, Gasser, T, Gehlen, M, Gilfillan, D, Gkritzalis, T, Gregor, L, Gruber, N, Harris, I, Hartung, K, Haverd, V, Houghton, RA, Ilyina, T, Jain, AK, Joetzjer, E, Kadono, K, Kato, E, Kitidis, V, Korsbakken, JI, Landschützer, P, Lefèvre, N, Lenton, A, Lienert, S, Liu, Z, Lombardozzi, D, Marland, G, Metzl, N, Munro, DR, Nabel, JEMS, Nakaoka, S-I, Niwa, Y, O'Brien, K, Ono, T, Palmer, PI, Pierrot, D, Poulter, B, Resplandy, L, Robertson, E, Rödenbeck, C, Schwinger, J, Séférian, R, Skjelvan, I, Smith, AJP, Sutton, AJ, Tanhua, T, Tans, PP, Tian, H, Tilbrook, B, van der Werf, G, Vuichard, N, Walker, AP, Wanninkhof, R, Watson, AJ, Willis, D, Wiltshire, AJ, Yuan, W, Yue, X, Zaehle, S.** 2020. Global carbon budget 2020. *Earth System Science Data* **12**(4): 3269–3340. DOI: <http://dx.doi.org/10.5194/essd-12-3269-2020>.
- Gafar, NA, Eyre, BD, Schulz, KG.** 2018. A conceptual model for projecting coccolithophorid growth, calcification and photosynthetic carbon fixation rates in response to global ocean change. *Frontiers in Marine Science* **4**(433): 1–18. DOI: <http://dx.doi.org/10.3389/fmars.2017.00433>.
- Gangstø, R, Gehlen, M, Schneider, B, Bopp, L, Aumont, O, Joos, F.** 2008. Modeling the marine aragonite cycle: Changes under rising carbon dioxide and its role in shallow water CaCO₃ dissolution. *Biogeosciences* **5**(4): 1057–1072. DOI: <http://dx.doi.org/10.5194/bg-5-1057-2008>.
- Gangstø, R, Joos, F, Gehlen, M.** 2011. Sensitivity of pelagic calcification to ocean acidification. *Biogeosciences* **8**(2): 433–458. DOI: <http://dx.doi.org/10.5194/bg-8-433-2011>.
- Gao, K, Beardall, J, Häder, DP, Hall-Spencer, JM, Gao, G, Hutchins, DA.** 2019. Effects of ocean acidification on marine photosynthetic organisms under the concurrent influences of warming, UV radiation and deoxygenation. *Frontiers in Marine Science* **6**(322): 1–18. DOI: <http://dx.doi.org/10.3389/fmars.2019.00322>.
- Gao, K, Zhang, Y, Häder, DP.** 2018. Individual and interactive effects of ocean acidification, global warming, and UV radiation on phytoplankton. *Journal of Applied Phycology* **30**(2): 743–759. DOI: <http://dx.doi.org/10.1007/s10811-017-1329-6>.
- Garcia, HE, Boyer, TP, Locarnini, RA, Antonov, JI, Mishonov, AV, Baranova, OK, Zweng, MM, Reagan, JR, Johnson, DR, Levitus, S.** 2013. *World Ocean Atlas 2013. Volume 3, Dissolved oxygen, apparent oxygen utilization, and oxygen saturation*. Silver Spring, MD: National Oceanographic Data Center, Ocean Climate Laboratory. DOI: <http://dx.doi.org/10.7289/V5XG9P2W>.
- Garcia, NS, Fu, FX, Breene, CL, Yu, EK, Bernhardt, PW, Mulholland, MR, Hutchins, DA.** 2013. Combined

- effects of CO₂ and light on large and small isolates of the unicellular N₂-fixing cyanobacterium *Crocosphaera watsonii* from the western tropical Atlantic Ocean. *European Journal of Phycology* **48**(1): 128–139. DOI: <http://dx.doi.org/10.1080/09670262.2013.773383>.
- Gattuso, JP, Epitalon, JM, Lavigne, H, Orr, J.** 2019. seacarb: Seawater carbonate chemistry. R-package version 3.2.12. Available at <http://CRAN.R-project.org/package=seacarb>. Accessed 11 February 2021.
- Gehlen, M, Bopp, L, Emprin, N, Aumont, O, Heinze, C, Ragueneau, O.** 2006. Reconciling surface ocean productivity, export fluxes and sediment composition in a global biogeochemical ocean model. *Biogeosciences* **3**(4): 521–537. DOI: <http://dx.doi.org/10.5194/bg-3-521-2006>.
- Geider, RJ, MacIntyre, HL, Kana, TM.** 1998. A dynamic regulatory model of phytoplanktonic acclimation to light, nutrients, and temperature. *Limnology and Oceanography* **43**(4): 679–694. DOI: <http://dx.doi.org/10.4319/lo.1998.43.4.0679>.
- Godrijan, J, Drapeau, D, Balch, WM.** 2020. Mixotrophic uptake of organic compounds by coccolithophores. *Limnology and Oceanography* **65**(6): 1410–1421. DOI: <http://dx.doi.org/10.1002/lno.11396>.
- Gregg, WW, Casey, NW.** 2007. Modeling coccolithophores in the global oceans. *Deep Sea Research Part II: Topical Studies in Oceanography* **54**(5): 447–477. DOI: <http://dx.doi.org/10.1016/j.dsr2.2006.12.007>.
- Gruber, N.** 2011. Warming up, turning sour, losing breath: Ocean biogeochemistry under global change. *Philosophical Transactions of the Royal Society A: Mathematical, Physical and Engineering Sciences* **369**(1943): 1980–1996. DOI: <http://dx.doi.org/10.1098/rsta.2011.0003>.
- Haidar, AT, Thierstein, HR.** 2001. Coccolithophore dynamics off Bermuda (N. Atlantic). *Deep Sea Research Part II: Topical Studies in Oceanography* **48**(8): 1925–1956. DOI: [http://dx.doi.org/10.1016/S0967-0645\(00\)00169-7](http://dx.doi.org/10.1016/S0967-0645(00)00169-7).
- Hare, CE, Leblanc, K, DiTullio, GR, Kudela, RM, Zhang, Y, Lee, PA, Riseman, S, Hutchins, DA.** 2007. Consequences of increased temperature and CO₂ for phytoplankton community structure in the Bering Sea. *Marine Ecology Progress Series* **352**: 9–16. DOI: <http://dx.doi.org/10.3354/meps07182>.
- Harvey, BP, Gwynn-Jones, D, Moore, PJ.** 2013. Meta-analysis reveals complex marine biological responses to the interactive effects of ocean acidification and warming. *Ecology and Evolution* **3**(4): 1016–1030. DOI: <http://dx.doi.org/10.1002/ece3.516>.
- Hauck, J, Völker, C, Wang, T, Hoppema, M, Losch, M, Wolf-Gladrow, DA.** 2013. Seasonally different carbon flux changes in the Southern Ocean in response to the southern annular mode. *Global Biogeochemical Cycles* **27**(4): 1236–1245. DOI: <http://dx.doi.org/10.1002/2013GB004600>.
- Hauck, J, Völker, C, Wolf-Gladrow, DA, Laufkötter, C, Vogt, M, Aumont, O, Bopp, L, Buitenhuis, ET, Doney, SC, Dunne, J, Gruber, N, Hashioka, T, John, J, Quéré, CL, Lima, ID, Nakano, H, Séférian, R, Totterdell, I.** 2015. On the Southern Ocean CO₂ uptake and the role of the biological carbon pump in the 21st century. *Global Biogeochemical Cycles* **29**(9): 1451–1470. DOI: <http://dx.doi.org/10.1002/2015GB005140>.
- Haunost, M, Riebesell, U, D'Amore, F, Kelting, O, Bach, LT.** 2021. Influence of the calcium carbonate shell of coccolithophores on ingestion and growth of a dinoflagellate predator. *Frontiers in Marine Science* **8**: 738. DOI: <http://dx.doi.org/10.3389/fmars.2021.664269>.
- Hennon, GMM, Quay, P, Morales, RL, Swanson, LM, Virginia Armbrust, E.** 2014. Acclimation conditions modify physiological response of the diatom *Thalassiosira pseudonana* to elevated CO₂ concentrations in a nitrate-limited chemostat. *Journal of Phycology* **50**(2): 243–253. DOI: <http://dx.doi.org/10.1111/jpy.12156>.
- Henson, SA, Sanders, R, Madsen, E, Morris, PJ, Le Moigne, F, Quartly, GD.** 2011. A reduced estimate of the strength of the ocean's biological carbon pump. *Geophysical Research Letters* **38**(4): 1–5. DOI: <http://dx.doi.org/10.1029/2011GL046735>.
- Hermoso, M.** 2015. Control of ambient pH on growth and stable isotopes in phytoplanktonic calcifying algae. *Paleoceanography* **30**(8): 1100–1112. DOI: <http://dx.doi.org/10.1002/2015PA002844>.
- Holt, J, Allen, JI, Anderson, TR, Brewin, R, Butenschön, M, Harle, J, Huse, G, Lehodey, P, Lindemann, C, Memery, L, Salihoglu, B, Senina, I, Yool, A.** 2014. Challenges in integrative approaches to modelling the marine ecosystems of the North Atlantic: Physics to fish and coasts to ocean. *Progress in Oceanography* **129**: 285–313. DOI: <http://dx.doi.org/10.1016/j.pocean.2014.04.024>.
- Hopkins, J, Balch, WM.** 2018. A new approach to estimating coccolithophore calcification rates from space. *Journal of Geophysical Research: Biogeosciences* **123**(5): 1447–1459. DOI: <http://dx.doi.org/10.1002/2017JG004235>.
- Hoppe, CJM, Flintrop, CM, Rost, B.** 2018. The Arctic picoeukaryote *Micromonas pusilla* benefits synergistically from warming and ocean acidification. *Biogeosciences* **15**(14): 4353–4365. DOI: <http://dx.doi.org/10.5194/bg-15-4353-2018>.
- Hoppe, CJM, Langer, G, Rost, B.** 2011. *Emiliania huxleyi* shows identical responses to elevated pCO₂ in TA and DIC manipulations. *Journal of Experimental Marine Biology and Ecology* **406**(1–2): 54–62. DOI: <http://dx.doi.org/10.1016/j.jembe.2011.06.008>.
- Ihnken, S, Roberts, S, Beardall, J.** 2011. Differential responses of growth and photosynthesis in the marine diatom *Chaetoceros muelleri* to CO₂ and light availability. *Phycologia* **50**(2): 182–193. DOI: <http://dx.doi.org/10.2216/10-11.1>.
- Irion, S, Christaki, U, Berthelot, H, L'helguen, S, Jardillier, L.** 2021. Small phytoplankton contribute greatly to CO₂-fixation after the diatom bloom in

- the Southern Ocean. *The ISME Journal*: 1–14. DOI: <http://dx.doi.org/10.1038/s41396-021-00915-z>.
- Irwin, AJ, Finkel, ZV, Schofield, OME, Falkowski, PG.** 2006. Scaling-up from nutrient physiology to the size-structure of phytoplankton communities. *Journal of Plankton Research* **28**(5): 459–471. DOI: <http://dx.doi.org/10.1093/plankt/fbi148>.
- Jansen, H, Wolf-Gladrow, DA.** 2001. Carbonate dissolution in copepod guts: A numerical model. *Marine Ecology Progress Series* **221**: 199–207. DOI: <http://dx.doi.org/10.3354/meps221199>.
- Jin, X, Gruber, N, Dunne, JP, Sarmiento, JL, Armstrong, RA.** 2006. Diagnosing the contribution of phytoplankton functional groups to the production and export of particulate organic carbon, CaCO₃, and opal from global nutrient and alkalinity distributions. *Global Biogeochemical Cycles* **20**(2): 1–17. DOI: <http://dx.doi.org/10.1029/2005GB002532>.
- Karakuş, O, Völker, C, Iversen, M, Hagen, W, Gladrow, DW, Fach, B, Hauck, J.** 2021. Modeling the impact of macrozooplankton on carbon export production in the Southern Ocean. *Journal of Geophysical Research: Oceans* **126**(12): e2021JC017315. DOI: <http://dx.doi.org/10.1029/2021JC017315>.
- Kelly, MW, Griffiths, JS.** 2021. Selection experiments in the sea: What can experimental evolution tell us about how marine life will respond to climate change? *The Biological Bulletin* **241**: 30–42. DOI: <http://dx.doi.org/10.1086/715109>.
- Kim, H, Spivack, AJ, Menden-Deuer, S.** 2013. pH alters the swimming behaviors of the raphidophyte *Heterosigma akashiwo*: Implications for bloom formation in an acidified ocean. *Harmful Algae* **26**: 1–11. DOI: <http://dx.doi.org/10.1016/j.hal.2013.03.004>.
- Klaas, C, Archer, DE.** 2002. Association of sinking organic matter with various types of mineral ballast in the deep sea: Implications for the rain ratio. *Global Biogeochemical Cycles* **16**(4): 63–1–63–14. DOI: <http://dx.doi.org/10.1029/2001GB001765>.
- Kottmeier, DM, Rokitta, SD, Rost, B.** 2016. Acidification, not carbonation, is the major regulator of carbon fluxes in the coccolithophore. *Emiliania huxleyi*. *New Phytologist* **211**: 126–137. DOI: <http://dx.doi.org/10.1111/nph.13885>.
- Kottmeier, DM, Rokitta, SD, Tortell, PD, Rost, B.** 2014. Strong shift from HCO₃⁻ to CO₂ uptake in *Emiliania huxleyi* with acidification: New approach unravels acclimation versus short-term pH effects. *Photosynthesis Research* **121**(2–3): 265–275. DOI: <http://dx.doi.org/10.1007/s11120-014-9984-9>.
- Kranz, SA, Dieter, S, Richter, KU, Rost, B.** 2009. Carbon acquisition by *Trichodesmium*: The effect of pCO₂ and diurnal changes. *Limnology and Oceanography* **54**(2): 548–559. DOI: <http://dx.doi.org/10.4319/lo.2009.54.2.0548>.
- Krug, S, Schulz, K, Riebesell, U.** 2011. Effects of changes in carbonate chemistry speciation on *Coccolithus braarudii*: A discussion of coccolithophorid sensitivities. *Biogeosciences* **8**: 771–777. DOI: <http://dx.doi.org/10.5194/bg-8-771-2011>.
- Krumhardt, KM, Lovenduski, NS, Freeman, NM, Bates, NR.** 2016. Apparent increase in coccolithophore abundance in the subtropical North Atlantic from 1990 to 2014. *Biogeosciences* **13**(4): 1163–1177. DOI: <http://dx.doi.org/10.5194/bg-13-1163-2016>.
- Krumhardt, KM, Lovenduski, NS, Iglesias-Rodriguez, MD, Kleypas, JA.** 2017. Coccolithophore growth and calcification in a changing ocean. *Progress in Oceanography* **159**: 276–295. DOI: <http://dx.doi.org/10.1016/j.pocean.2017.10.007>.
- Krumhardt, KM, Lovenduski, NS, Long, MC, Levy, M, Lindsay, K, Moore, JK, Nissen, C.** 2019. Coccolithophore growth and calcification in an acidified ocean: Insights from Community Earth System Model simulations. *Journal of Advances in Modeling Earth Systems* **11**(5): 1418–1437. DOI: <http://dx.doi.org/10.1029/2018MS001483>.
- Kvale, KF, Meissner, KJ, Keller, DP, Eby, M, Schmittner, A.** 2015. Explicit planktic calcifiers in the University of Victoria Earth System Climate Model, Version 2.9. *Atmosphere-Ocean* **53**(3): 332–350. DOI: <http://dx.doi.org/10.1080/07055900.2015.1049112>.
- Kwiatkowski, L, Torres, O, Bopp, L, Aumont, O, Chamberlain, M, Christian, JR, Dunne, JP, Gehlen, M, Ilyina, T, John, JG, Lenton, A, Li, H, Lovenduski, NS, Orr, JC, Palmieri, J, Santana-Falcón, Y, Schwinger, J, Séférian, R, Stock, CA, Tagliabue, A, Takano, Y, Tjiputra, J, Toyama, K, Tsujino, H, Watanabe, M, Yamamoto, A, Yool, A, Ziehn, T.** 2020. Twenty-first century ocean warming, acidification, deoxygenation, and upper-ocean nutrient and primary production decline from CMIP6 model projections. *Biogeosciences* **17**(13): 3439–3470. DOI: <http://dx.doi.org/10.5194/bg-17-3439-2020>.
- Langer, G, Geisen, M, Baumann, KH, Kläs, J, Riebesell, U, Thoms, S, Young, JR.** 2006. Species-specific responses of calcifying algae to changing seawater carbonate chemistry. *Geochemistry, Geophysics, Geosystems* **7**(9): 1–12. DOI: <http://dx.doi.org/10.1029/2005GC001227>.
- Langer, G, Nehrke, G, Probert, I, Ly, J, Ziveri, P.** 2009. Strain-specific responses of *Emiliania huxleyi* to changing seawater carbonate chemistry. *Biogeosciences* **6**(11): 2637–2646. DOI: <http://dx.doi.org/10.5194/bg-6-2637-2009>.
- Lauvset, SK, Key, RM, Olsen, A, van Heuven, S, Velo, A, Lin, X, Schirnack, C, Kozyr, A, Tanhua, T, Hoppema, M, Jutterström, S, Steinfeldt, R, Jeansson, E, Ishii, M, Perez, FF, Suzuki, T, Watelet, S.** 2016. A new global interior ocean mapped climatology: The 1° × 1° GLODAP version 2. *Earth System Science Data* **8**(2): 325–340. DOI: <http://dx.doi.org/10.5194/essd-8-325-2016>.
- Le Quéré, C, Harrison, SP, Colin Prentice, I, Buitenhuis, ET, Aumont, O, Bopp, L, Claustre, H, Cotrim Da Cunha, L, Geider, R, Giraud, X, Klaas, C, Kohfeld, KE, Legendre, L, Manizza, M, Platt, T, Rivkin, RB, Sathyendranath, S, Uitz, J, Watson, AJ, Wolf-**

- Gladrow, D.** 2005. Ecosystem dynamics based on plankton functional types for global ocean biogeochemistry models. *Global Change Biology* **11**: 2016–2040. DOI: <http://dx.doi.org/10.1111/j.1365-2486.2005.1004.x>.
- Leblanc, K, Arstegui, J, Armand, L, Assmy, P, Beker, B, Bode, A, Breton, E, Cornet, V, Gibson, J, Gosselin, M-P, Kopczynska, E, Marshall, H, Peloquin, J, Piontkovski, S, Poulton, AJ, Quéguiner, B, Schiebel, R, Shipe, R, Stefels, J, van Leeuwe, MA, Varela, M, Widdicombe, C, Yallop, M.** 2012. A global diatom database—Abundance, biovolume and biomass in the world ocean. *Earth System Science Data* **4**(1): 149–165. DOI: <http://dx.doi.org/10.5194/essd-4-149-2012>.
- Lee, K.** 2001. Global net community production estimated from the annual cycle of surface water total dissolved inorganic carbon. *Limnology and Oceanography* **46**(6): 1287–1297. DOI: <http://dx.doi.org/10.4319/lo.2001.46.6.1287>.
- Li, F, Fan, J, Hu, L, Beardall, J, Xu, J.** 2019. Physiological and biochemical responses of *Thalassiosira weissflogii* (diatom) to seawater acidification and alkalization. *ICES Journal of Marine Science* **76**(6): 1850–1859. DOI: <http://dx.doi.org/10.1093/icesjms/fsz028>.
- Li, W, Gao, K, Beardall, J.** 2012. Interactive effects of ocean acidification and nitrogen-limitation on the diatom *Phaeodactylum tricornutum*. *PLoS One* **7**(12): e51590. DOI: <http://dx.doi.org/10.1371/journal.pone.0051590>.
- Li, W, Yang, Y, Li, Z, Xu, J, Gao, K.** 2017. Effects of seawater acidification on the growth rates of the diatom *Thalassiosira (Conticribra) weissflogii* under different nutrient, light, and UV radiation regimes. *Journal of Applied Phycology* **29**(1): 133–142. DOI: <http://dx.doi.org/10.1007/s10811-016-0944-y>.
- Litchman, E, Klausmeier, CA, Schofield, OM, Falkowski, PG.** 2007. The role of functional traits and trade-offs in structuring phytoplankton communities: Scaling from cellular to ecosystem level. *Ecology Letters* **10**(12): 1170–1181. DOI: <http://dx.doi.org/10.1111/j.1461-0248.2007.01117.x>.
- Maat, DS, Crawford, KJ, Timmermans, KR, Brussaard, CPD, Wommack, KE.** 2014. Elevated CO₂ and phosphate limitation favor *Micromonas pusilla* through stimulated growth and reduced viral impact. *Applied and Environmental Microbiology* **80**(10): 3119–3127. DOI: <http://dx.doi.org/10.1128/AEM.03639-13>.
- Marañón, E, Cermeño, P, López-Sandoval, DC, Rodríguez-Ramos, T, Sobrino, C, Huete-Ortega, M, Blanco, JM, Rodríguez, J.** 2013. Unimodal size scaling of phytoplankton growth and the size dependence of nutrient uptake and use. *Ecology Letters* **16**(3): 371–379. DOI: <http://dx.doi.org/10.1111/ele.12052>.
- Margalef, R.** 1978. Life-forms of phytoplankton as survival alternatives in an unstable environment. *Oceanologica Acta* **1**(4): 493–509.
- Mayers, KMJ, Poulton, AJ, Bidle, K, Thamtracoln, K, Schieler, B, Giering, SLC, Wells, SR, Tarran GA, Mayor, D, Johnson, M, Riebesell, U, Larsen, A, Vardi, A, Harvey, EL.** 2020. The possession of coccoliths fails to deter microzooplankton grazers. *Frontiers in Marine Science* **7**: 976. DOI: <http://dx.doi.org/10.3389/fmars.2020.569896>.
- Meyer, J, Riebesell, U.** 2015. Reviews and syntheses: Responses of coccolithophores to ocean acidification: A meta-analysis. *Biogeosciences* **12**(6): 1671–1682. DOI: <http://dx.doi.org/10.5194/bg-12-1671-2015>.
- Middelburg, JJ.** 2019. *Marine carbon biogeochemistry—A primer for earth system scientists*, in Lohmann, G, Mysak, LA, Notholt, J, Rabassa, J, Unnithan, V eds., *Springer briefs in earth system sciences*. Berlin, Germany: Springer Open. DOI: <http://dx.doi.org/10.1007/978-3-030-10822-9>.
- Milliman, JD, Troy, PJ, Balch, WM, Adams, AK, Li, YH, Mackenzie, FT.** 1999. Biologically mediated dissolution of calcium carbonate above the chemical lysocline? *Deep Sea Research Part I: Oceanographic Research Papers* **46**(10): 1653–1669. DOI: [http://dx.doi.org/10.1016/S0967-0637\(99\)00034-5](http://dx.doi.org/10.1016/S0967-0637(99)00034-5).
- Monteiro, FM, Bach, LT, Brownlee, C, Bown, P, Rickaby, REM, Poulton, AJ, Tyrrell, T, Beaufort, L, Dutkiewicz, S, Gibbs, S, Gutowska, MA, Lee, R, Riebesell, U, Young, J, Ridgwell, A.** 2016. Why marine phytoplankton calcify. *Science Advances* **2**(7): e1501822. DOI: <http://dx.doi.org/10.1126/sciadv.1501822>.
- Moore, JK, Fu, W, Primeau, F, Britten, GL, Lindsay, K, Long, M, Doney, SC, Mahowald, N, Hoffman, F, Randerson, JT.** 2018. Sustained climate warming drives declining marine biological productivity. *Science* **359**(6380): 1139–1143. DOI: <http://dx.doi.org/10.1126/science.aao6379>.
- Moriarty, R, O'Brien, TD.** 2013. Distribution of mesozooplankton biomass in the global ocean. *Earth System Science Data* **5**(1): 45–55. DOI: <http://dx.doi.org/10.5194/essd-5-45-2013>.
- Mucci, A.** 1983. The solubility of calcite and aragonite in seawater at various salinities, temperatures, and one atmosphere total pressure. *American Journal of Science* **283**(7): 780–799. DOI: <http://dx.doi.org/10.2475/ajs.283.7.780>.
- Müller, MN, Trull, TW, Hallegraeff, GM.** 2015. Differing responses of three Southern Ocean *Emiliania huxleyi* ecotypes to changing seawater carbonate chemistry. *Marine Ecology Progress Series* **531**: 81–90. DOI: <http://dx.doi.org/10.3354/meps11309>.
- Nelson, DM, Tréguer, P, Brzezinski, MA, Leynaert, A, Quéguiner, B.** 1995. Production and dissolution of biogenic silica in the ocean: Revised global estimates, comparison with regional data and relationship to biogenic sedimentation. *Global Biogeochemical Cycles* **9**(3): 359–372. DOI: <http://dx.doi.org/10.1029/95GB01070>.
- Nielsen, MV.** 1997. Growth, dark respiration and photosynthetic parameters of the coccolithophorid

- Emiliana huxleyi* (Prymnesiophyceae) acclimated to different day length-irradiance combinations. *Journal of Phycology* **33**(5): 818–822. DOI: <http://dx.doi.org/10.1111/j.0022-3646.1997.00818.x>.
- Nissen, C, Vogt, M, Münnich, M, Gruber, N, Haumann, FA.** 2018. Factors controlling coccolithophore biogeography in the Southern Ocean. *Biogeosciences* **15**(22): 6997–7024. DOI: <http://dx.doi.org/10.5194/bg-15-6997-2018>.
- O'Brien, CJ, Peloquin, JA, Vogt, M, Heinle, M, Gruber, N, Ajani, P, Andrulleit, H, Arístegui, J, Beaufort, L, Estrada, M, Karentz, D, Koczyńska, E, Lee, R, Poulton, AJ, Pritchard, T, Widdicombe, C.** 2013. Global marine plankton functional type biomass distributions: Coccolithophores. *Earth System Science Data* **5**(2): 259–276. DOI: <http://dx.doi.org/10.5194/essd-5-259-2013>.
- Orr, J, Epitalon, JM.** 2015. Improved routines to model the ocean carbonate system: Mocsy 2.0. *Biogeosciences* **8**: 485–499. DOI: <http://dx.doi.org/10.5194/gmd-8-485-2015>.
- Paasche, E.** 2001. A review of the coccolithophorid *Emiliana huxleyi* (Prymnesiophyceae), with particular reference to growth, coccolith formation, and calcification-photosynthesis interactions. *Phycologia* **40**(6): 503–529. DOI: <http://dx.doi.org/10.2216/i0031-8884-40-6-503.1>.
- Palevsky, HI, Doney, SC.** 2018. How choice of depth horizon influences the estimated spatial patterns and global magnitude of ocean carbon export flux. *Geophysical Research Letters* **45**(9): 4171–4179. DOI: <http://dx.doi.org/10.1029/2017GL076498>.
- Panassa, E, Santana-Casiano, JM, González-Dávila, M, Hoppema, M, van Heuven, SMAC, Völker, C, Wolf-Gladrow, D, Hauck, J.** 2018. Variability of nutrients and carbon dioxide in the Antarctic Intermediate Water between 1990 and 2014. *Ocean Dynamics* **68**(3): 295–308. DOI: <http://dx.doi.org/10.1007/s10236-018-1131-2>.
- Pančić, M, Hansen, PJ, Tammilehto, A, Lundholm, N.** 2015. Resilience to temperature and pH changes in a future climate change scenario in six strains of the polar diatom *Fragilariopsis cylindrus*. *Biogeosciences* **12**(14): 4235–4244. DOI: <http://dx.doi.org/10.5194/bg-12-4235-2015>.
- Paul, AJ, Bach, LT.** 2020. Universal response pattern of phytoplankton growth rates to increasing CO₂. *New Phytologist* **228**(6): 1710–1716. DOI: <http://dx.doi.org/10.1111/nph.16806>.
- Peter, KH, Sommer, U.** 2012. Phytoplankton cell size: Intra- and interspecific effects of warming and grazing. *PLoS One* **7**(11): 1–9. DOI: <http://dx.doi.org/10.1371/journal.pone.0049632>.
- Petrou, K, Baker, KG, Nielsen, DA, Hancock, AM, Schulz, KG, Davidson, AT.** 2019. Acidification diminishes diatom silica production in the Southern Ocean. *Nature Climate Change* **9**(10): 781–786. DOI: <http://dx.doi.org/10.1038/s41558-019-0557-y>.
- Petrou, K, Kranz, SA, Trimborn, S, Hassler, CS, Ameijeiras, SB, Sackett, O, Ralph, PJ, Davidson, AT.** 2016. Southern Ocean phytoplankton physiology in a changing climate. *Journal of Plant Physiology* **203**: 135–150. DOI: <http://dx.doi.org/10.1016/j.jplph.2016.05.004>.
- Pierella Karlusich, JJ, Bowler, C, Biswas, H.** 2021. Carbon dioxide concentration mechanisms in natural populations of marine diatoms: Insights from Tara Oceans. *Frontiers in Plant Science* **12**: 659. DOI: <http://dx.doi.org/10.3389/fpls.2021.657821>.
- Pinkerton, MH, Boyd, PW, Deppeler, S, Hayward, A, Höfer, J, Moreau, S.** 2021. Evidence for the impact of climate change on primary producers in the Southern Ocean. *Frontiers in Ecology and Evolution* **9**: 134. DOI: <http://dx.doi.org/10.3389/fevo.2021.592027>.
- Poloczanska, ES, Burrows, MT, Brown, CJ, Garca Molinos, J, Halpern, BS, Hoegh-Guldberg, O, Kappel, CV, Moore, PJ, Richardson, AJ, Schoeman, DS, Sydeman, WJ.** 2016. Responses of marine organisms to climate change across oceans. *Frontiers in Marine Science* **3**: 62. DOI: <http://dx.doi.org/10.3389/fmars.2016.00062>.
- Pond, DW, Harris, RP, Brownlee, C.** 1995. A microinjection technique using a pH-sensitive dye to determine the gut pH of *Calanus helgolandicus*. *Marine Biology* **123**(1): 75–79. DOI: <http://dx.doi.org/10.1007/BF00350325>.
- Poulton, AJ, Adey, TR, Balch, WM, Holligan, PM.** 2007. Relating coccolithophore calcification rates to phytoplankton community dynamics: Regional differences and implications for carbon export. *Deep Sea Research Part II: Topical Studies in Oceanography* **54**(5): 538–557. DOI: <http://dx.doi.org/10.1016/j.dsr2.2006.12.003>.
- Raitzsch, M, Gattuso, JP.** 2020. ScarFace—Seacarb calculations with R Shiny user interface. DOI: <http://dx.doi.org/10.5281/zenodo.4153455>.
- Reinfelder, JR.** 2011. Carbon concentrating mechanisms in eukaryotic marine phytoplankton. *Annual Review of Marine Science* **3**(1): 291–315. DOI: <http://dx.doi.org/10.1146/annurev-marine-120709-142720>.
- Riebesell, U, Bach, LT, Bellerby, RG, Monsalve, JRB, Boxhammer, T, Czerny, J, Larsen, A, Ludwig, A, Schulz, KG.** 2017. Competitive fitness of a predominant pelagic calcifier impaired by ocean acidification. *Nature Geoscience* **10**: 19–24. DOI: <http://dx.doi.org/10.1038/NGEO2854>.
- Riebesell, U, Zondervan, I, Rost, B, Tortell, PD, Zeebe, RE, Morel, FMM.** 2000. Reduced calcification of marine plankton in response to increased atmospheric CO₂. *Nature* **407**(6802): 364. DOI: <http://dx.doi.org/10.1038/35030078>.
- Riegman, R, Stolte W, Noordeeloos, AAM, Slezak, D.** 2000. Nutrient uptake and alkaline phosphatase (EC 3:1:3:1) activity of *Emiliana huxleyi* (Prymnesiophyceae) during growth under N and P limitation in continuous cultures. *Journal of Phycology* **36**: 87–96. DOI: <http://dx.doi.org/10.1046/j.1529-8817.2000.99023.x>.

- Rigual-Hernández, AS, Sánchez-Santos, JM, Eriksen, R, Moy, AD, Sierro, FJ, Flores, JA, Abrantes, F, Bostock, H, Nodder, SD, González-Lanchas, A, Trull, TW.** 2020. Limited variability in the phytoplankton *Emiliania huxleyi* since the pre-industrial era in the Subantarctic Southern Ocean. *Anthropocene* **31**: 100254. DOI: <http://dx.doi.org/10.1016/j.ancene.2020.100254>.
- Rivero-Calle, S, Gnanadesikan, A, Del Castillo, CE, Balch, WM, Guikema, SD.** 2015. Multidecadal increase in North Atlantic coccolithophores and the potential role of rising CO₂. *Science* **350**(6267): 1533–1537. DOI: <http://dx.doi.org/10.1126/science.aaa8026>.
- Rost, B, Riebesell, U.** 2004. Coccolithophores and the biological pump: Responses to environmental changes, in Thierstein, HR, Young, JR eds., *Coccolithophores*. Berlin, Germany: Springer: 99–125. DOI: http://dx.doi.org/10.1007/978-3-662-06278-4_5.
- Rost, B, Zondervan, I, Wolf-Gladrow, D.** 2008. Sensitivity of phytoplankton to future changes in ocean carbonate chemistry: Current knowledge, contradictions and research directions. *Marine Ecology Progress Series* **373**: 227–237. DOI: <http://dx.doi.org/10.3354/meps07776>.
- Sabine, CL, Key, RM, Feely, RA, Greeley, D.** 2002. Inorganic carbon in the Indian Ocean: Distribution and dissolution processes. *Global Biogeochemical Cycles* **16**(4): 15-1–15-18. DOI: <http://dx.doi.org/10.1029/2002GB001869>.
- Sallée, JB, Pellichero, V, Akhoudas, C, Pauthenet, E, Vignes, L, Schmidtko, S, Garabato, AN, Sutherland, P, Kuusela, M.** 2021. Summertime increases in upper-ocean stratification and mixed-layer depth. *Nature* **591**(7851): 592–598. DOI: <http://dx.doi.org/10.1038/s41586-021-03303-x>.
- Sarmiento, JL, Dunne, J, Gnanadesikan, A, Key, RM, Matsumoto, K, Slater, R.** 2002. A new estimate of the CaCO₃ to organic carbon export ratio. *Global Biogeochemical Cycles* **16**(4): 54-1–54-12. DOI: <http://dx.doi.org/10.1029/2002GB001919>.
- Sarthou, G, Timmermans, KR, Blain, S, Tréguer, P.** 2005. Growth physiology and fate of diatoms in the ocean: A review. *Journal of Sea Research* **53**(1): 25–42. DOI: <http://dx.doi.org/10.1016/j.seares.2004.01.007>.
- Schlitzer, R.** 2000. Applying the adjoint method for biogeochemical modeling: Export of particulate organic matter in the world ocean. *Geophysical Monograph—American Geophysical Union* **114**: 107–124.
- Schlüter, L, Lohbeck, KT, Gutowska, MA, Gröger, JP, Riebesell, U, Reusch, TBH.** 2014. Adaptation of a globally important coccolithophore to ocean warming and acidification. *Nature Climate Change* **4**(11): 1024–1030. DOI: <http://dx.doi.org/10.1038/NCLIMATE2379>.
- Schneider, B, Bopp, L, Gehlen, M, Segschneider, J, Frölicher, TL, Cadule, P, Friedlingstein, P, Doney, SC, Behrenfeld, MJ, Joos, F.** 2008. Climate-induced interannual variability of marine primary and export production in three global coupled climate carbon cycle models. *Biogeosciences* **5**(2): 597–614. DOI: <http://dx.doi.org/10.5194/bg-5-597-2008>.
- Schourup-Kristensen, V, Sidorenko, D, Wolf-Gladrow, DA, Völker, C.** 2014. A skill assessment of the biogeochemical model REcoM2 coupled to the Finite Element Sea Ice–Ocean Model (FESOM 1.3). *Geoscientific Model Development* **7**(6): 2769–2802. DOI: <http://dx.doi.org/10.5194/gmd-7-2769-2014>.
- Seifert, M, Hauck, J.** 2022. Cascading effects augment the direct impact of CO₂ on phytoplankton growth in a biogeochemical model, links to model results. Zenodo. DOI: <http://dx.doi.org/10.5281/zenodo.6674793>.
- Seifert, M, Rost, B, Trimborn, S, Hauck, J.** 2020. Meta-analysis of multiple driver effects on marine phytoplankton highlights modulating role of pCO₂. *Global Change Biology* **26**(12): 6787–6804. DOI: <http://dx.doi.org/10.1111/gcb.15341>.
- Sett, S, Bach, LT, Schulz, KG, Koch-Klavsén, S, Lebrato, M, Riebesell, U.** 2014. Temperature modulates coccolithophorid sensitivity of growth, photosynthesis and calcification to increasing seawater pCO₂. *PLoS One* **9**(2): e88308. DOI: <http://dx.doi.org/10.1371/journal.pone.0088308>.
- Shi, D, Hong, H, Su, X, Liao, L, Chang, S, Lin, W.** 2019. The physiological response of marine diatoms to ocean acidification: differential roles of seawater pCO₂ and pH. *Journal of Phycology* **55**(3): 521–533. DOI: <http://dx.doi.org/10.1111/jpy.12855>.
- Shutler, J, Land, PE, Brown, CW, Findlay, HS, Donlon, CJ, Medland, M, Snooke, R, Blackford, JC.** 2013. Coccolithophore surface distributions in the North Atlantic and their modulation of the air-sea flux of CO₂ from 10 years of satellite Earth observation data. *Biogeosciences* **10**(4): 2699–2709. DOI: <http://dx.doi.org/10.5194/bg-10-2699-2013>.
- Sidorenko, D, Wang, Q, Danilov, S, Schröter, J.** 2011. FESOM under coordinated ocean-ice reference experiment forcing. *Ocean Dynamics* **61**(7): 881–890. DOI: <http://dx.doi.org/10.1007/s10236-011-0406-7>.
- Sinha, B, Buitenhuis, ET, Quéré, CL, Anderson, TR.** 2010. Comparison of the emergent behavior of a complex ecosystem model in two ocean general circulation models. *Progress in Oceanography* **84**(3): 204–224. DOI: <http://dx.doi.org/10.1016/j.pocean.2009.10.003>.
- Spungin, D, Berman-Frank, I, Levitan, O.** 2014. *Trichodesmium's* strategies to alleviate phosphorus limitation in the future acidified oceans. *Environmental Microbiology* **16**(6): 1935–1947. DOI: <http://dx.doi.org/10.1111/1462-2920.12424>.
- Steele, M, Morley, R, Ermold, W.** 2001. PHC: A global ocean hydrography with a high-quality Arctic Ocean. *Journal of Climate* **14**(9): 2079–2087. DOI: [http://dx.doi.org/10.1175/1520-0442\(2001\)014<2079:PAAGOH>2.0.CO;2](http://dx.doi.org/10.1175/1520-0442(2001)014<2079:PAAGOH>2.0.CO;2).

- Stoecker, DK, Hansen, PJ, Caron, DA, Mitra, A.** 2017. Mixotrophy in the Marine Plankton. *Annual Review of Marine Science* **9**(1): 311–335.
- Sugie, K, Yoshimura, T.** 2013. Effects of pCO₂ and iron on the elemental composition and cell geometry of the marine diatom *Pseudo-nitzschia pseudodelicatissima* (Bacillariophyceae). *Journal of Phycology* **49**(3): 475–488. DOI: <http://dx.doi.org/10.1111/jpy.12054>.
- Sugie, K, Yoshimura, T.** 2016. Effects of high CO₂ levels on the ecophysiology of the diatom *Thalassiosira weissflogii* differ depending on the iron nutritional status. *ICES Journal of Marine Science* **73**(3): 680–692. DOI: <http://dx.doi.org/10.1093/icesjms/fsv259>.
- Sulpis, O, Jeansson, E, Dinauer, A, Lauvset, SK, Mid-delburg, JJ.** 2021. Calcium carbonate dissolution patterns in the ocean. *Nature Geoscience* **14**: 423–428. DOI: <http://dx.doi.org/10.1038/s41561-021-00743-y>.
- Tatters, AO, Roleda, MY, Schnetzer, A, Fu, F, Hurd, CL, Boyd, PW, Caron, DA, Lie, AAY, Hoffmann, LJ, Hutchins, DA.** 2013. Short- and long-term conditioning of a temperate marine diatom community to acidification and warming. *Philosophical Transactions of the Royal Society B: Biological Sciences* **368**(1627): 20120437. DOI: <http://dx.doi.org/10.1098/rstb.2012.0437>.
- Terrats, L, Claustre, H, Cornec, M, Mangin, A, Neukermans, G.** 2020. Detection of coccolithophore blooms with BioGeoChemical-Argo floats. *Geophysical Research Letters* **47**(23): e2020GL090559. DOI: <http://dx.doi.org/10.1029/2020GL090559>.
- Tortell, PD, Payne, CD, Li, Y, Trimborn, S, Rost, B, Smith, WO, Riesselman, C, Dunbar, RB, Sedwick, P, DiTullio, GR.** 2008. CO₂ sensitivity of Southern Ocean phytoplankton. *Geophysical Research Letters* **35**(4): 1–5. DOI: <http://dx.doi.org/10.1029/2007GL032583>.
- Tréguer, PJ, De La Rocha, CL.** 2013. The world ocean silica cycle. *Annual Review of Marine Science* **5**(1): 477–501. DOI: <http://dx.doi.org/10.1146/annurev-marine-121211-172346>.
- Tréguer, PJ, Sutton, JN, Brzezinski, M, Charette, MA, Devries, T, Dutkiewicz, S, Ehlert, C, Hawkings, J, Leynaert, A, Liu, SM, Llopis Monferrer, N, López-Acosta, M, Maldonado, M, Rahman, S, Ran, L, Rouxel, O.** 2021. Reviews and syntheses: The biogeochemical cycle of silicon in the modern ocean. *Biogeosciences* **18**(4): 1269–1289. DOI: <http://dx.doi.org/10.5194/bg-18-1269-2021>.
- Trimborn, S, Brenneis, T, Sweet, E, Rost, B.** 2013. Sensitivity of Antarctic phytoplankton species to ocean acidification: Growth, carbon acquisition, and species interaction. *Limnology and Oceanography* **58**(3): 997–1007. DOI: <http://dx.doi.org/10.4319/lo.2013.58.3.0997>.
- Tsujino, H, Urakawa, S, Nakano, H, Small, RJ, Kim, WM, Yeager, S, Danabasoglu, G, Suzuki, T, Bamber, JL, Bentsen, M, Böning, CW, Bozec, A, Chassignet, EP, Curchitser, E, Dias, FB, Durack, PJ, Griffies, SM, Harada, Y, Ilicak, M, Josey, SA, Kobayashi, C, Kobayashi, S, Komuro, Y, Large, WG, Sommer, JL, Marsland, SJ, Masina, S, Scheinert, M, Tomita, H, Valdivieso, M, Yamazaki, D.** 2018. JRA-55 based surface dataset for driving ocean–sea-ice models (JRA55-do). *Ocean Modelling* **130**: 79–139. DOI: <http://dx.doi.org/10.1016/j.ocemod.2018.07.002>.
- Vallina, SM, Ward, BA, Dutkiewicz, S, Follows, MJ.** 2014. Maximal feeding with active prey-switching: A kill-the-winner functional response and its effect on global diversity and biogeography. *Progress in Oceanography* **120**: 93–109. DOI: <http://dx.doi.org/10.1016/j.pocean.2013.08.001>.
- Wang, Q, Danilov, S, Sidorenko, D, Timmermann, R, Wekerle, C, Wang, X, Jung, T, Schröter, J.** 2014. The Finite Element Sea Ice–Ocean Model (FESOM) v. 1.4: Formulation of an ocean general circulation model. *Geoscientific Model Development* **7**(2): 663–693. DOI: <http://dx.doi.org/10.5194/gmd-7-663-2014>.
- White, E, Hoppe, CJM, Rost, B.** 2020. The Arctic picoeukaryote *Micromonas pusilla* benefits from ocean acidification under constant and dynamic light. *Biogeosciences* **17**(3): 635–647. DOI: <http://dx.doi.org/10.5194/bg-17-635-2020>.
- White, MM, Waller, JD, Lubelczyk, LC, Drapeau, DT, Bowler, BC, Balch, WM, Fields, DM.** 2018. Coccolith dissolution within copepod guts affects fecal pellet density and sinking rate. *Scientific Reports* **8**(1): 1–6. DOI: <http://dx.doi.org/10.1038/s41598-018-28073-x>.
- Wolf, KKE, Hoppe, CJM, Rost, B.** 2018. Resilience by diversity: Large intraspecific differences in climate change responses of an Arctic diatom. *Limnology and Oceanography* **63**(1): 397–411. DOI: <http://dx.doi.org/10.1002/lno.10639>.
- Wu, Y, Campbell, DA, Irwin, AJ, Suggett, DJ, Finkel, ZV.** 2014. Ocean acidification enhances the growth rate of larger diatoms. *Limnology and Oceanography* **59**(3): 1027–1034. DOI: <http://dx.doi.org/10.4319/lo.2014.59.3.1027>.
- Wyatt, T.** 2014. Margalef's mandala and phytoplankton bloom strategies. *Deep Sea Research Part II: Topical Studies in Oceanography* **101**: 32–49. DOI: <http://dx.doi.org/10.1016/j.dsr2.2012.12.006>.
- Yamanaka, Y, Tajika, E.** 1996. The role of the vertical fluxes of particulate organic matter and calcite in the oceanic carbon cycle: Studies using an ocean biogeochemical general circulation model. *Global Biogeochemical Cycles* **10**(2): 361–382. DOI: <http://dx.doi.org/10.1029/96GB00634>.
- Zhang, Y, Fu, F, Hutchins, DA, Gao, K.** 2019. Combined effects of CO₂ level, light intensity, and nutrient availability on the coccolithophore *Emiliania huxleyi*. *Hydrobiologia* **842**: 127–141. DOI: <http://dx.doi.org/10.1007/s10750-019-04031-0>.
- Zondervan, I.** 2007. The effects of light, macronutrients, trace metals and CO₂ on the production of calcium

carbonate and organic carbon in coccolithophores—A review. *Deep Sea Research Part II: Topical Studies in Oceanography* **54**(5): 521–537. DOI: <http://dx.doi.org/10.1016/j.dsr2.2006.12.004>.

Zondervan, I, Rost, B, Riebesell, U. 2002. Effect of CO₂ concentration on the PIC/POC ratio in the coccolithophore *Emiliana huxleyi* grown under light-limiting conditions and different daylengths.

Journal of Experimental Marine Biology and Ecology **272**: 55–70. DOI: [http://dx.doi.org/10.1016/S0022-0981\(02\)00037-0](http://dx.doi.org/10.1016/S0022-0981(02)00037-0).

Zondervan, I, Zeebe, RE, Rost, B, Riebesell, U. 2001. Decreasing marine biogenic calcification: A negative feedback on rising atmospheric pCO₂. *Global Biogeochemical Cycles* **15**(2): 507–516. DOI: <http://dx.doi.org/10.1029/2000GB001321>.

How to cite this article: Seifert, M, Nissen, C, Rost, B, Hauck, J. 2022. Cascading effects augment the direct impact of CO₂ on phytoplankton growth in a biogeochemical model. *Elementa: Science of the Anthropocene* 10(1). DOI: <https://doi.org/10.1525/elementa.2021.00104>

Domain Editor-in-Chief: Jody W. Deming, University of Washington, Seattle, WA, USA

Associate Editor: Jean-Éric Tremblay, Université Laval, Québec, Canada

Knowledge Domain: Ocean Science

Published: September 16, 2022 **Accepted:** July 29, 2022 **Submitted:** November 9, 2021

Copyright: © 2022 The Author(s). This is an open-access article distributed under the terms of the Creative Commons Attribution 4.0 International License (CC-BY 4.0), which permits unrestricted use, distribution, and reproduction in any medium, provided the original author and source are credited. See <http://creativecommons.org/licenses/by/4.0/>.

